Volume 54
Number 20
28 May 2025
Pages 7957-8360

# Dalton Transactions

An international journal of inorganic chemistry

rsc.li/dalton

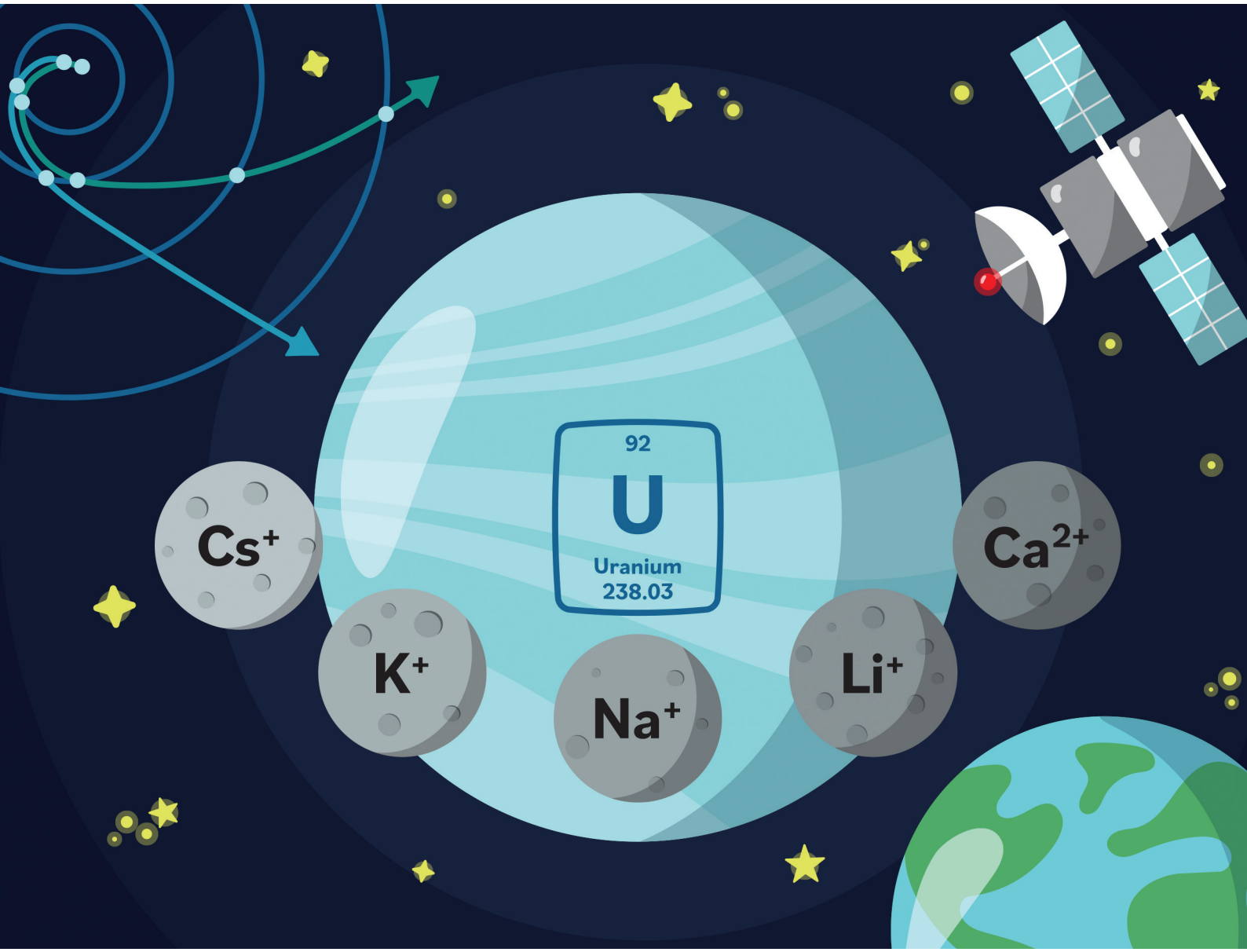


ISSN 1477-9226

ROYAL SOCIETY OF CHEMISTRY

**PAPER**

Tori Z. Forbes, James D. Blakemore *et al.*

Macrocyclic control of electron transfer to high valent uranium in heterobimetallic complexes

Dalton Transactions

ROYAL SOCIETY OF CHEMISTRY

PAPER

View Article Online
View Journal | View Issue

Check for updates

Cite this: *Dalton Trans.*, 2025, **54**, 8061

# Macrocyclic control of electron transfer to high valent uranium in heterobimetallic complexes†

Amit Kumar,‡§[a] Riddhi R. Golwankar, ‡[a] Mikaela M. F. Pyrch, ¶[b] Fynn L. Cooper,[a] Grant A. Arehart,[a] Korey P. Carter, [b] Allen G. Oliver, [c] Victor W. Day,[a] Tori Z. Forbes *[b] and James D. Blakemore *[a]

Received 20th December 2024,
Accepted 12th March 2025

DOI: 10.1039/d4dt03503h

rsc.li/dalton

The redox properties of the uranyl ion, $UO_2^{2+}$, influence the chemistry required for nuclear fuel reprocessing, but little spectroscopic insight is available to support design strategies for influencing the redox properties of uranium complexes. Here, structural studies with X-ray diffraction analysis, electrochemical methods, and Raman spectroscopy have been used to examine one strategy for influencing uranyl redox chemistry, namely co-encapsulation of $UO_2^{2+}$ and secondary metal cations ($Cs^+$, $Rb^+$, $K^+$, $Na^+$, $Li^+$, and $Ca^{2+}$) in macrocyclic ligands. Two ligands are compared in this work that differ in the denticities of their secondary cation binding sites (pentadentate *vs.* hexadentate), enabling direct quantification of influences on the redox and vibrational properties of the uranyl moiety. The $U^{VI}/U^{V}$ thermodynamic reduction potential is correlated with the effective Lewis acidity of the secondary metal cations; solid-state and solution-phase Raman spectra show that this effect can be attributed to electrostatics that effectively drive diminished electron donation to uranium in adducts of more strongly Lewis acidic cations. The heterogeneous electron transfer (ET) rates for $U^{VI}/U^{V}$ redox processes, however, depend on both the strength of cation binding in the macrocycles and the Lewis acidity of the cations, suggesting opportunities for molecular design in development of reagents for nuclear fuel reprocessing/separations.

Open Access Article. Published on 12 March 2025. Downloaded on 6/5/2026 2:38:04 PM.
This article is licensed under a Creative Commons Attribution-NonCommercial 3.0 Unported Licence.

## Introduction

Nuclear power based on fission of uranium is an important source of low-carbon electricity, but unresolved issues related to fuel recycling and waste management have hampered further development of this remarkable global energy resource.[1] Virtually all nuclear fuel recycling schemes involve redox-driven changes in actinide solubility and speciation that are used to separate useful uranium from other components of irradiated "used" fuel.[2] This is true of both established fuel reprocessing chemistries, like the Plutonium Uranium Redox EXtraction (PUREX) process,[3] and next-generation approaches involving totally non-aqueous conditions[4] and/or molten salt chemistries[5] to achieve isolation of useful uranium for further use in power generation.

The chemistry of uranium under most conditions is dominated by the uranyl dication, $UO_2^{2+}$.[6] This species forms quite readily under oxidizing and/or aqueous conditions, including those found in the conventional fuel recycling chemistry of the PUREX process.[3] $UO_2^{2+}$ features high-valent uranium in the formal +VI oxidation state, but under most conditions, this species is rather difficult to reduce. This is consistent with the $E°(U^{VI}/U^{V})$ value of 0.16 V *vs.* the standard hydrogen electrode (SHE), in that under nearly all conditions,[7] electro-reduction of $UO_2^{2+}$ is challenging and associated with significant overpotentials. Indeed, electrolysis of $UO_2^{2+}$-containing solutions can lead to significant parasitic reactions.[8] Considering that reduction of $UO_2^{2+}$ is required for fuel reprocessing and that $UO_2^{2+}$ redox chemistry is also important in environmental speciation of uranium, understanding and ultimately controlling the redox chemistry of uranium could be useful for development of next-generation nuclear fuel recycling schemes.

Inspired by work in transition metal chemistry,[9] a portion of our interest in recent years has been drawn to the strategy of using effectively Lewis acidic secondary metal cations for tuning the redox chemistry of uranium.[10] In our work, we have used macrocyclic ligands to prepare complexes that can incorporate a

[a]*Department of Chemistry, University of Kansas, 1567 Irving Hill Road, Lawrence, Kansas 66045, USA. E-mail: blakemore@ku.edu*
[b]*Department of Chemistry, University of Iowa, Iowa City, Iowa 52242, USA. E-mail: tori-forbes@uiowa.edu*
[c]*Department of Chemistry and Biochemistry, University of Notre Dame, Notre Dame, Indiana 46556, USA*

†Electronic supplementary information (ESI) available. CCDC 2344717–2344726. For ESI and crystallographic data in CIF or other electronic format see DOI: https://doi.org/10.1039/d4dt03503h

‡These authors contributed equally to this work.

§Current address: Heraeus Precious Metals, 15524 Carmenita Road, Santa Fe Springs, California 90670, USA.

¶Current address: Department of Chemistry, University of California, Berkeley, Berkeley, California 94720, USA.

Open Access Article. Published on 12 March 2025. Downloaded on 6/5/2026 2:38:04 PM.
This article is licensed under a Creative Commons Attribution-NonCommercial 3.0 Unported Licence.

diverse range of secondary metal cations, including lanthanide cations,[10–14] and found for the case of $UO_2^{2+}$ complexes that the $U^{VI}/U^{V}$ potential could be tuned reliably by incorporation of cations. In that work, the Lewis acidity of the cations, quantified through the p$K_a$ values of the corresponding metal aqua complexes, served as a useful descriptor for the achievable reduction-potential modulation, revealing a relationship of −61 ± 9 mV/p$K_a$ for $U^{VI}/U^{V}$ cycling. Hallmarks of this relationship have been observed in several other classes of compounds,[15,16] beyond ours based on macrocyclic ligands. Prior work has tended to focus, however, on systems in which uranyl oxo ligands serve as bridging atoms to secondary metal cations. The groups of Arnold[17] and Mazzanti,[18] have mapped the properties of complexes of this type, in particular, finding that cations stabilize lower-valent forms of uranium (Fig. 1). Borane electrophiles can be used as well, as shown by Sarsfield,[19] Hayton,[20] and others, representing a particularly attractive set of reagents for stabilizing U(v). Blakemore and co-workers have recently been exploring boranes, including $BPh_3$, electrode-driven uranyl functionalization as well.[21,22]

However, little spectroscopic data is available to help interpret the origins of redox tuning effects. Quantitative insights into the influence of secondary cations on actinide metal centers could be impactful for developing predictive models and design of new ligands. Along this line, the role of macrocyclic structure in achieving optimal tuning behavior has also not received the attention that it deserves, but we have anticipated that the macrocycle-promoted structural placement of secondary metal cations could influence cation-driven tuning.[23–25] Such concepts are sensible in the general context of Lewis acid–base chemistry, but to the best of our knowledge, no studies in macrocyclic chemistry have directly interrogated how the structure of a supporting ligand framework modulates heterometallic redox tuning. Agapie and co-workers have shown, however, that non-macrocyclic ligand changes are quite impactful in iron oxo cluster chemistry.[15] We thus hypothesized that the supramolecular fit of the secondary cations in ligands would influence the redox chemistry, building on the known propensity of macrocyclic ligands to override natural bonding preferences.[26] Given the broad utility of Raman spectroscopy in actinide chemistry,[27] we anticipated that Raman data for macrocyclic systems would afford insights relevant to development of controlled uranyl redox chemistry and next-generation nuclear fuel recycling strategies. Data examining cation-induced redox effects from the perspective of Raman spectroscopy would also usefully build on established correlations between first- and second-sphere interactions and observed vibrational frequencies.[28–31]

Here, we report a comparison of the structural, spectroscopic, and electrochemical properties of two related families of heterobimetallic complexes (**$L^5UO_2M$** and **$L^6UO_2M$**) that incorporate secondary redox-inactive metal ions **M** (where **M** is $Cs^+$, $Rb^+$, $K^+$, $Na^+$, $Li^+$, or $Ca^{2+}$, see Fig. 2). The consequences of binding the secondary metal ions have been mapped in order to delineate the influences of cation Lewis acidity, macrocyclic ligand structure, and relevant cation association constants on the vibrational and redox properties of the uranyl motif. X-ray diffraction analysis (XRD) revealed that the coordination properties of the secondary metal ion binding site (penta- *vs.* hexadentate) controls placement of the cations relative to the uranium center in the complexes, resulting in unique tuning sensitivities for both reduction potentials and symmetric U–O vibrational frequencies. However, the electron transfer rate is optimized only by balancing the influences of both Lewis acidity and macrocyclic structure, resulting in unique "volcano plots" for each ligand explored here that can be understood to arise from the molecular design features implemented in this work.

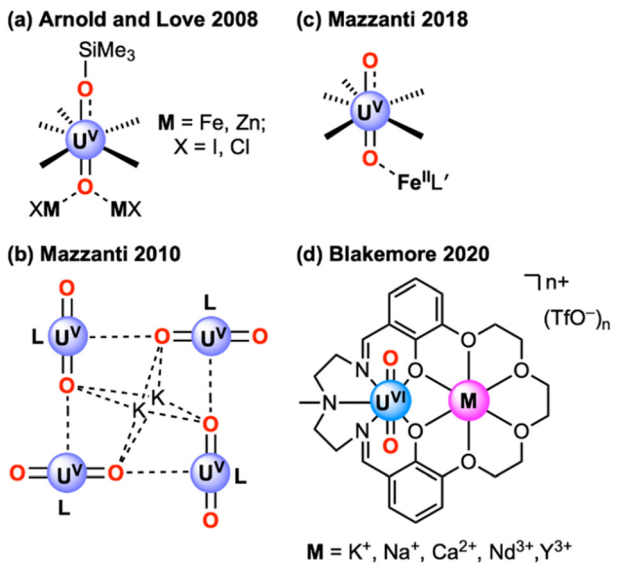


Fig. 1 Structures of complexes in which secondary cations influence the measured or apparent redox properties of the uranyl motif. From ref. 17*a*, 18 and 10.

## Results

### Characterization and comparison of the macrocyclic ligands

Two ligands were used in this work to support assembly of two unique families of heterobimetallic complexes. Ligands of the

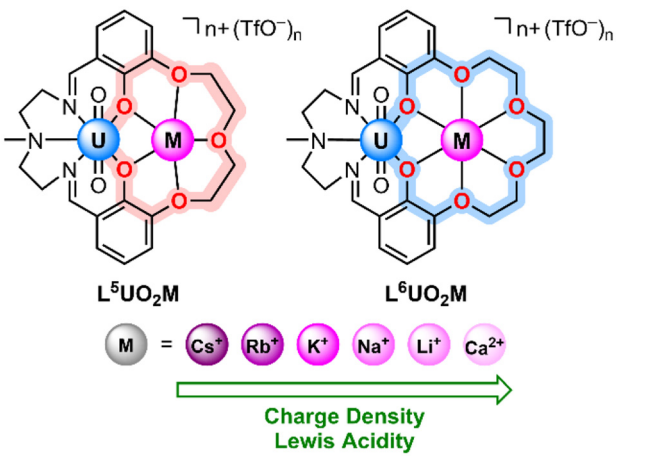


Fig. 2 Heterobimetallic complexes of the uranyl dication.


This journal is © The Royal Society of Chemistry 2025

Open Access Article. Published on 12 March 2025. Downloaded on 6/5/2026 2:38:04 PM.
This article is licensed under a Creative Commons Attribution-NonCommercial 3.0 Unported Licence.

type used here were developed by Reinhoudt and co-workers in the late 1980s[32] and subsequently elaborated upon by Vigato and co-workers.[33] The ligands themselves, denoted as $\mathbf{L^5H_2}$ and $\mathbf{L^6H_2}$, feature a similar Schiff-base site in both cases that supports $UO_2^{2+}$ binding (Fig. 2). Importantly, each ligand offers a second binding site, based upon a polyether motif, for incorporation of secondary metal cations. $\mathbf{L^5H_2}$ provides a 15-crown-5-like pentadentate moiety for cation binding, while $\mathbf{L^6H_2}$ offers a larger 18-crown-6-like hexadentate moiety. These polyether sites were designed to be proximal to the site for uranyl binding, encouraging interaction of the metal cations with the uranyl motif not by direct interaction with the terminal oxo ligands but rather *via* the phenoxide donor groups of the macrocycle. $\mathbf{L^5H_2}$ has not previously been used to prepare heterobimetallic complexes, but we previously utilized $\mathbf{L^6H_2}$ to prepare a small set of four crystallographically characterized heterobimetallic complexes.[10]

Building on this experience, we recognized that monometallic uranyl complexes of the macrocyclic ligands, denoted $\mathbf{L^5UO_2}$ and $\mathbf{L^6UO_2}$, would need to be prepared in order to access divergent synthesis of a range of bimetallic complexes. To access these monometallic complexes, we prepared precursors in which the neutral ligands $\mathbf{L^5H_2}$ and $\mathbf{L^6H_2}$ were templated and stabilized by coordination to barium, affording species denoted **BaPenta** and **BaHexa**, respectively (see Experimental section in ESI† for details).[10,33] $^1$H and $^{19}$F nuclear magnetic resonance data confirmed the successful isolation of both these known precursors as desired (Fig. S1 and S2;† fluorine derived from triflate counteranions).

XRD analysis carried out on suitable crystals of **BaPenta** revealed, however, that this complex prefers to crystallize as a 2 : 1 $\mathbf{L^5H_2}$ : $Ba^{2+}$ adduct in which $Ba^{2+}$ is sandwiched between the crown-ether-like sites of the $\mathbf{L^5H_2}$ units (Fig. 3a and Fig. S164–166†) with the triflate counteranions in the outer sphere. The $Ba^{2+}$ center adopts the high coordination number (C.N.) of 10 by interacting with all ten macrocyclic O-atoms present in the two equivalents of $\mathbf{L^5H_2}$ present in the structure; this is sensible given the large ionic radius of 1.52 Å for $Ba^{2+}$ with C.N. = 10.[34] The formulation of the macrocycles as $\mathbf{L^5H_2}$ units (rather than their deprotonated analogues) was confirmed by $^1$H NMR spectroscopy (Fig. S1†), as well as by successful location and free refinement of the phenol-associated H protons. These protons appear acidified by $Ba^{2+}$ coordination, however, with the nearby imine N-atoms assisting in formation of strong [N–H···O] H-bonds.

The structure of **BaPenta** was compared with the available prior structure of **BaHexa**.[10] The structure of **BaHexa** revealed a 1 : 1 $\mathbf{L^6H_2}$ : Ba adduct, with the $Ba^{2+}$ ion coordinated to the six macrocyclic O-atoms of $\mathbf{L^6H_2}$. $Ba^{2+}$ adopts the C.N. of 10 by binding two triflate counteranions in the inner sphere, both in the $\kappa^2$-mode, in line with the large size of $Ba^{2+}$ and the apparent preference of this dication to adopt C.N. = 10 in both 18- and 15-crown systems. Perhaps the most important difference between the structures is that the $Ba^{2+}$ ion does not bind near the centroid of either crown ether cavity to which it is bound in **BaPenta**. The phenomenon of $Ba^{2+}$ being significantly displaced above the crown ether cavities was quantified by the $\psi_M$ parameter, defined as the root mean square deviation of the Ba atom above the mean plane defined by the crown oxygen atoms (Table S12†). The $\psi_M$ values for **BaPenta** and **BaHexa** are 1.570 and 0.048 Å, respectively. This finding is attributable to the larger size of the 18-crown-6-like cavity in $\mathbf{L^6H_2}$, which enables $Ba^{2+}$ to nestle comfortably into the site (Fig. S168†). The separation between two phenoxide O atoms (O1···O2) is smaller for **BaPenta** than **BaHexa** (3.328(4) Å *vs.* 3.641(3) Å), consistent with the presence of a more constricted and planar cavity that results in displacement of $Ba^{2+}$ above the plane of the 15-crown-5-like site.

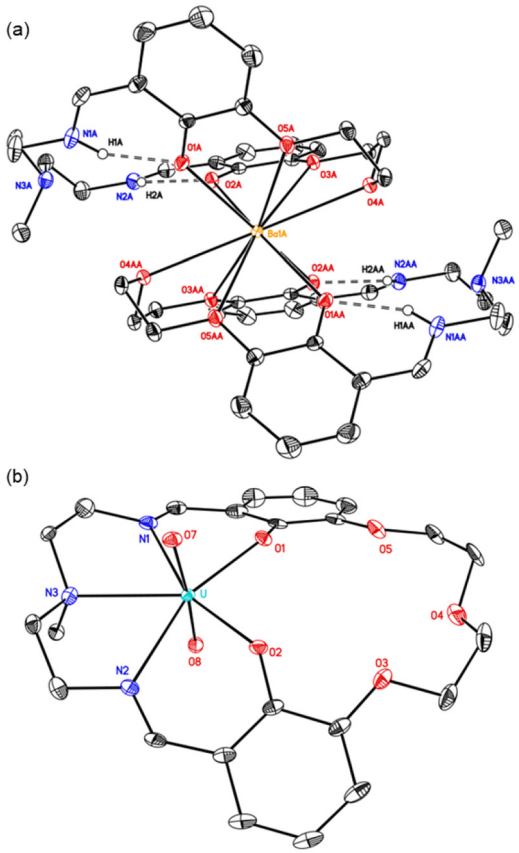


**Fig. 3** Solid-state structures from XRD of (a) **BaPenta** and (b) $\mathbf{L^5UO_2}$. Outer sphere triflate counteranions and co-crystallized diethyl ether molecules associated with **BaPenta**, a co-crystallized $CH_3CN$ molecule associated with $\mathbf{L^5UO_2}$, minor components of disorder, and all hydrogen atoms omitted for clarity. Displacement ellipsoids are shown at 20% probability level. The phenolic protons H1A, H2A, H1AA, and H2AA were included as independent atoms that were freely refined in the final structural model.

Using literature methods, **BaPenta** and **BaHexa** were converted into the monometallic uranyl-containing complexes $\mathbf{L^5UO_2}$ and $\mathbf{L^6UO_2}$.[10,33] $^1$H NMR and elemental analysis confirmed isolation of the desired complexes in each case (see Experimental section in ESI† for details). Single crystals of $\mathbf{L^5UO_2}$ were grown for XRD analysis, and the resulting structure confirmed coordination of $UO_2^{2+}$ in the Schiff base site of

Open Access Article. Published on 12 March 2025. Downloaded on 6/5/2026 2:38:04 PM. This article is licensed under a Creative Commons Attribution-NonCommercial 3.0 Unported Licence.

the macrocycle, similar to the case of $\mathbf{L^6UO_2}$ as revealed in a prior structure.[10] Both the new structure of $\mathbf{L^5UO_2}$ and the older structure of $\mathbf{L^6UO_2}$ confirm that the crown ether-like sites are poised to bind secondary metal cations (Fig. S173†). The crown ether moieties in $\mathbf{L^5UO_2}$ and $\mathbf{L^6UO_2}$ appear distinctive in each case, however, with significantly greater co-planarity of the oxygen atoms in $\mathbf{L^5UO_2}$. As in our prior work,[11] the $\omega_{crown}$ parameter was used to quantify the planarity of the crown-ether O-atoms (see Table 1). The value of this parameter is 0.055 for $\mathbf{L^5UO_2}$ and 0.358 for $\mathbf{L^6UO_2}$ (Table S14†), consistent with the notion that the O-atoms in $\mathbf{L^5UO_2}$ form a more compact platform of donor atoms *on top of which* secondary metal cations could bind. This contrasts with the case of $\mathbf{L^6UO_2}$, which features a crown site with sufficient flexibility and inter-O-atom spacing to *encapsulate* secondary cations.

### *In situ* synthesis and characterization of the heterobimetallic complexes

With the monometallic complexes $\mathbf{L^5UO_2}$ and $\mathbf{L^6UO_2}$ in hand, we turned to the preparation of the corresponding groups of heterobimetallic complexes. For the work reported here, we studied monovalent alkali metal cations ($Cs^+$, $Rb^+$, $K^+$, $Na^+$, $Li^+$) and a single divalent ion ($Ca^{2+}$), as these cations represent a wide acidity range of around four orders of magnitude, as estimated by consideration of the p$K_a$ values of corresponding metal aqua complexes. This series also features cations that could be reasonably anticipated to display satisfactory binding behavior with 15-crown-5 or 18-crown-6 moieties. We found that $\mathbf{L^5UO_2}$ or $\mathbf{L^6UO_2}$ could be treated with 1 equiv. of the desired metal triflate salt in acetonitrile, resulting in a virtually instantaneous change in the color of the solution that is concomitant with cation binding in the crown moieties. $^1$H NMR spectra for all the complexes formed *in situ* displayed uniform and sensible shifts in the positions of resonances that were consistent in all cases with binding of the metal cations to the oxygen atoms of the crown-ether-like cavities (see ESI, pp. S15–S33†). Isolation of powdered samples was generally not pursued; instead, samples of the complexes were generated *in situ* as needed to execute the experimental work. Titration studies were also performed to measure the equilibrium constants for cation binding (*vide infra*), and these studies indicate generally tight capture of the cations in the crown moieties as anticipated from the NMR data.

Crystals of the adducts of $\mathbf{L^5UO_2}$ with $Li^+$, $Na^+$, and $Ca^{2+}$ suitable for X-ray diffraction analysis were grown in order to understand the structural properties of the complexes. Efforts were made to grow diffraction-quality crystals of $\mathbf{L^5UO_2K}$, $\mathbf{L^5UO_2Rb}$ and $\mathbf{L^5UO_2Cs}$, but none could be obtained; this could be due to the larger size of these cations.[34] To facilitate the needed comparisons, we have tabulated the structural data for structures in the $\mathbf{L^5UO_2M}$ and $\mathbf{L^6UO_2M}$ families in Table 1; structures of the complexes $\mathbf{L^6UO_2M}$ were previously

**Table 1** p$K_a$ values for $[M(H_2O)_m]^{n+}$ species, coordination numbers, Shannon ionic radius values, and selected bond lengths, interatomic distances, root mean square deviations ($\omega$), and displacements of atoms from defined planes ($\psi$) in heterobimetallic $UO_2^{2+}$ complexes

| Compound | $\mathbf{L^5UO_2Li}$ | $\mathbf{L^6UO_2Li}$ | $\mathbf{L^5UO_2Na}$ | $\mathbf{L^6UO_2Na}$ [b] | $\mathbf{L^5UO_2Ca}$ | $\mathbf{L^6UO_2Ca}$ [b] |
|---|---|---|---|---|---|---|
| p$K_a$ of $[\mathbf{M}(H_2O)_m]^{n+}$ | 13.8 | | 14.8 | | 12.6 | |
| C.N. of **M** | 6 | 6 | 6 | 7 | 7 | 9 |
| Ionic radius of **M** (Å)[a] | 0.76 | 0.76 | 1.02 | 1.12 | 1.06 | 1.18 |
| U···M (Å) | 3.489(4) | 3.304(10) | 3.605(2) | 3.668(3) | 3.690(1) | 3.923(1) |
| O1···O2 (Å) | 2.840(2) | 2.821(5) | 2.945(6) | 2.973(7) | 2.818(7) | 2.948(8) |
| U–O7$_{oxo}$ (Å) | 1.778(2) | 1.782(4) | 1.761(5) | 1.782(5) | 1.772(5) | 1.795(4) |
| U–O8$_{oxo}$ (Å) | 1.784(2) | 1.786(4) | 1.770(4) | 1.780(5) | 1.776(5) | 1.783(4) |
| U–O$_{oxo}$ (avg)[c] (Å) | 1.783(2) | 1.784(4) | 1.766(5) | 1.781(5) | 1.774(5) | 1.789(4) |
| U–O1$_{phenoxide}$ (Å) | 2.260(2) | 2.229(4) | 2.258(5) | 2.247(6) | 2.303(4) | 2.310(4) |
| U–O2$_{phenoxide}$ (Å) | 2.267(2) | 2.258(4) | 2.272(4) | 2.262(6) | 2.289(4) | 2.294(4) |
| U–O$_{phenoxide}$ (avg)[c] (Å) | 2.264(2) | 2.244(4) | 2.265(5) | 2.255(6) | 2.297(4) | 2.302(4) |
| U–N1$_{imine}$ (Å) | 2.555(2) | 2.550(5) | 2.543(6) | 2.538(8) | 2.520(6) | 2.471(6) |
| U–N2$_{imine}$ (Å) | 2.533(2) | 2.552(5) | 2.544(6) | 2.555(8) | 2.514(6) | 2.527(6) |
| U–N$_{imine}$ (avg)[c] (Å) | 2.544(2) | 2.551(5) | 2.544(6) | 2.547(8) | 2.517(6) | 2.499(6) |
| M–O1$_{phenoxide}$ (Å) | 2.216(4) | 2.119(10) | 2.403(5) | 2.584(7) | 2.398(5) | 2.525(4) |
| M–O2$_{phenoxide}$ (Å) | 2.288(4) | 2.086(10) | 2.444(4) | 2.435(8) | 2.419(4) | 2.715(4) |
| M–O$_{phenoxide}$ (avg)[c] (Å) | 2.252(4) | 2.103(10) | 2.424(5) | 2.510(8) | 2.409(5) | 2.620(4) |
| $\omega_{crown}$[d] (Å) | 0.367 | 0.701 | 0.366 | 0.717 | 0.332[h] | 0.609 |
| $\omega_{salben}$[e] (Å) | 0.095 | 0.051 | 0.112 | 0.157 | 0.116 | 0.203 |
| $\psi_U$[f] (Å) | 0.013 | 0.011 | 0.032 | 0.045 | 0.017 | 0.049 |
| $\psi_M$[g] (Å) | 0.585 | 0.440 | 0.838 | 0.652 | 1.123[h] | 0.322 |

[a] From ref. 34. [b] Structural data taken from ref. 10, CCDC 1960629 (ref. 36), and CCDC 1960628 (ref. 37). [c] Defined as the average interatomic distance between the noted metal and the relevant oxygen/nitrogen atoms. Stated estimated standard deviations (e.s.d.'s) on distances were taken as the largest of the individual values in the refined data for the independent bond distance. [d] Defined as the root mean square deviation (RMSD) of the positions of crown atoms O1, O2, O3, O4, and O5 from the mean plane of their positions for the species ligated by $\mathbf{L^5}$. O6 was included in the calculation for the species ligated by $\mathbf{L^6}$. [e] Defined as the root mean square deviation (RMSD) of O1, O2, N1, N2, and N3 from the mean plane of their positions. [f] Absolute value of the distance between U and the mean plane of O1, O2, N1, N2, and N3. [g] Absolute value of the distance between **M** and the mean plane of O1, O2, O3, O4, and O5 for the species ligated by $\mathbf{L^5}$. O6 was included in the calculation of the mean plane for the species ligated by $\mathbf{L^6}$. [h] Values are reported as the mean of the relevant individual values corresponding to two disordered orientations of O3 (O3′) and O4 (O4′) occupying the same volume of the asymmetric unit. Atom labels are consistent with those given in the raw crystallographic data (see pp. S178–S179† for details).

 This journal is © The Royal Society of Chemistry 2025

Open Access Article. Published on 12 March 2025. Downloaded on 6/5/2026 2:38:04 PM.
This article is licensed under a Creative Commons Attribution-NonCommercial 3.0 Unported Licence.

reported.[10] Our previous work, however, did not include structural data for the $\mathbf{L^6UO_2Li}$ complex; a new structure of this compound is reported here. In the course of our work, we explored various solvent systems and note that we obtained four different crystalline polymorphs of the $Na^+$ adduct of $\mathbf{L^5UO_2}$ (two of which are were found to be nearly isomorphous, see p. S157 and S169†) and two different crystalline polymorphs of the $Ca^{2+}$ adduct of $\mathbf{L^5UO_2}$. The structural metrics among the related cases were quite similar (see Tables S15, S16, and Fig. S184, S194, S199†), and thus we discuss below in detail only one of the structures for $\mathbf{L^5UO_2Na}$ and $\mathbf{L^5UO_2Ca}$ in each case that lack co-crystallized outer-sphere solvent. (One structure of $\mathbf{L^5UO_2Na}$ and the structure of $\mathbf{L^5UO_2Li}$ were also found to be nearly isomorphous. See p. S170.†)

In all cases, XRD analysis confirmed assembly of the desired $[UO_2(\mu_2\text{-}O_{phenoxide})_2\mathbf{M}^{n+}]$ cores. In the $\mathbf{L^5UO_2M}$ structures, the secondary metal cations ions are incorporated at the 15-crown-5-like site in all cases and ligated by the five macrocyclic O-atoms. Each of the structures with $Li^+$ and $Na^+$ feature one $\kappa^1$-triflate while the structure with $Ca^{2+}$ features two $\kappa^1$-triflates (see Fig. 4 and Fig. S174–S199†). $Li^+$ and $Na^+$ adopt C.N. = 6 despite their disparate ionic radii; this observation is in line with an analogous structure of the $\mathbf{L^6UO_2Na}$ complex[10] in which the secondary cation adopts C.N. = 7, suggesting that the size of the macrocyclic crown ether moieties, in both cases, influence the bonding preferences of the cations.

When $Li^+$ binds to the 18-crown-6-like site in $\mathbf{L^6UO_2Li}$, however, only five crown O-atoms interact with the cation, leaving one ethereal O-atom uncoordinated. The crown moiety is nonplanar in this structure, a feature attributable to the flexible nature of the crown moiety and a mismatch of the small $Li^+$ cation's ionic radius with the larger 18-crown-6 moiety (Fig. S174–S177†). The result is the formation of a dimer of the desired $\mathbf{L^6UO_2Li}$ species in the solid state, wherein an $O_{oxo}$ of the uranyl unit of one equivalent of $\mathbf{L^6UO_2Li}$ bridges to the $Li^+$ of the adjacent equivalent of the heterobimetallic species (see Fig. 5). Interestingly, the O3···O6 separation of 3.947 Å results in a nearly square array of oxygens ideal for binding of $Li^+$ at its center. This also allows O5 to coordinate above the plane but leaves a vacant *trans*-coordination site below the plane which can be accommodated by uranyl upon dimerization to give overall octahedral lithium centers. Despite the unique chemical environments of terminal oxo ligands O7 and O8, the U–O bond lengths are not different within the conventional 3σ criterion (see Table 1). This result is consistent with findings from Rissanen and co-workers in their characterization of a ditopic uranyl salophen complex.[35] However, we note that direct interactions of actinyl oxos with secondary metals are still rather rare, especially for U(VI), and thus we anticipate that the properties of $\mathbf{L^6UO_2Li}$ could be worthy of further investigation.

The U–$O_{oxo}$ distances in all the structures reported here are consistent with the retention of the U(VI) formal oxidation state. Unsurprisingly, the U–$O_{phenoxide}$ and U–$N_{imine}$ distances span narrow ranges, consistent with the uranyl motif being firmly bound in structurally similar sites in all cases for both

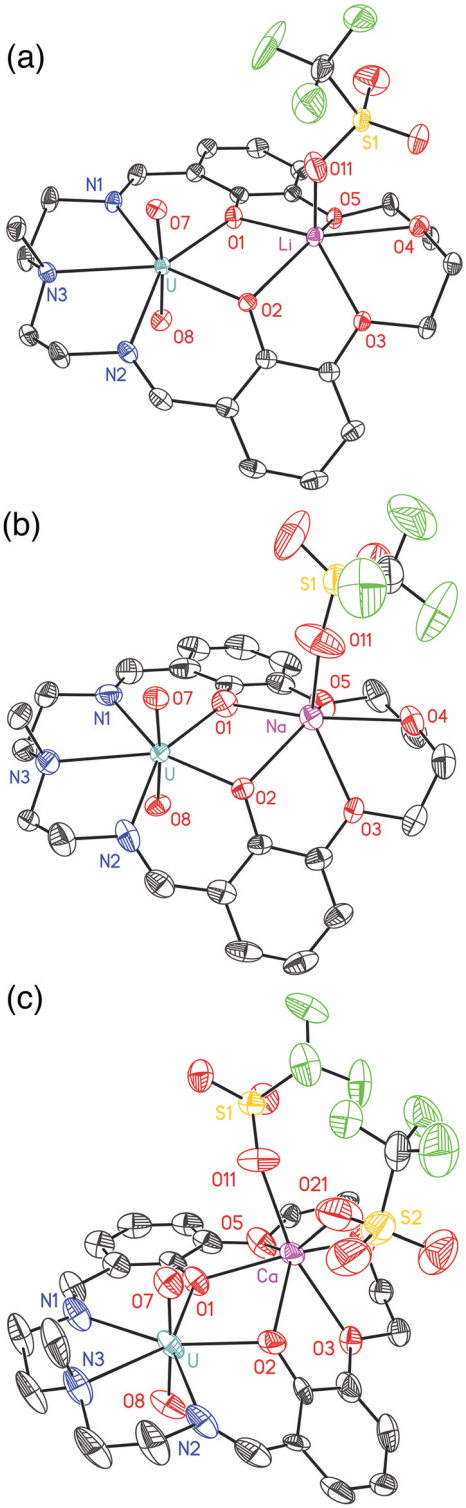


**Fig. 4** Solid-state structures (from XRD) of (a) $\mathbf{L^5UO_2Li}$, (b) $\mathbf{L^5UO_2Na}$, and (c) $\mathbf{L^5UO_2Ca}$. All hydrogen atoms, co-crystallized solvent molecules, and minor components of disorder are omitted for clarity. Displacement ellipsoids are shown at the 50% probability level.

the $\mathbf{L^5UO_2M}$ and $\mathbf{L^6UO_2M}$ species. This is in accord with the high degree of similarity for the uranyl sites in the corresponding monometallic species (see Fig. S173†). Also unsur-

Open Access Article. Published on 12 March 2025. Downloaded on 6/5/2026 2:38:04 PM.
This article is licensed under a Creative Commons Attribution-NonCommercial 3.0 Unported Licence.

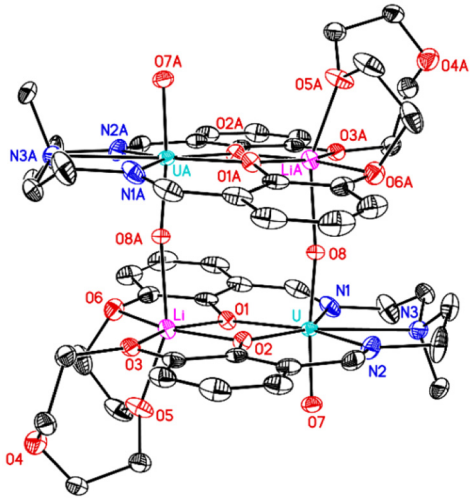


**Fig. 5** Solid-state dimeric structure from XRD of $\mathbf{L^6UO_2Li}$. All hydrogen atoms, outer-sphere triflate counteranions, and minor components of disorder about the U–N3 bond are omitted for clarity. Displacement ellipsoids are shown at the 50% probability level.

prisingly, comparing the structures of the $\mathbf{L^5UO_2M}$ and $\mathbf{L^6UO_2M}$ species reveals that the structures of the crown sites vary systematically across the series of complexes depending on the size and charge of the incorporated secondary cation. More specifically, the value of $\omega_{crown}$ increases in each case upon cation binding from the values measured for the monometallic complexes $\mathbf{L^5UO_2}$ and $\mathbf{L^6UO_2}$ of 0.055 and 0.358, respectively. Notably, the $\omega_{crown}$ parameter is *ca.* 2× larger in all cases for the 18-crown-6-containing derivatives, indicating that the larger crown behaves more flexibly in all cases. The $\psi_M$ parameters for the 15-crown-5-based derivatives is systematically greater than those found for the 18-crown-6-based derivatives. Consequently, the smaller ligand can be concluded to be less able to encapsulate the secondary cations both because of the relative smaller size of the ring in relation to the ionic radii of the secondary cations. As a result, the cations tend to bind above the plane of the macrocyclic ligand, a feature that could be enhanced by coordination of oxygen from triflate. In the larger 18-crown-6-based ligand, however, the cations can be encapsulated within the crown moiety as it is able to flex around incorporated cations. This tendency for the cations in the $\mathbf{L^5UO_2M}$ series to be bound above the macrocyclic plane contrasts with the positions of the U centers that are much closer to the macrocyclic plane and have an ideal fit with the Schiff-base moiety (quantified by $\psi_U$).

## Electrochemical studies

With the ability to prepare the heterobimetallic complexes in the $\mathbf{L^5UO_2M}$ or $\mathbf{L^6UO_2M}$ seriesm, we next explored the influence of the secondary metal cations on the thermodynamic $E_{1/2}(U^{VI}/U^{V})$ reduction potentials of the complexes. This could be achieved by adding one equivalent of the corresponding metal triflate salt to a solution of the desired monometallic uranyl complex (either $\mathbf{L^5UO_2}$ or $\mathbf{L^6UO_2}$) in $CH_3CN$ and subsequently recording cyclic voltammetry (CV) data. To begin, however, the CV profiles of $\mathbf{L^5UO_2}$ and $\mathbf{L^6UO_2}$ are unremarkable, displaying chemically reversible reduction at $E_{1/2} = -1.57$ V and −1.53 V *vs.* ferrocenium/ferrocene (denoted hereafter as $Fc^{+/0}$), respectively. The peak-to-peak separations ($\Delta E_p$) of 77 mV and 73 mV, respectively, are consistent with fast electron transfer (at 100 mV $s^{-1}$) for our configuration (see Table 2). The similar $E_{1/2}$ values in both cases are no doubt a consequence of the quite similar ligand environments of the uranyl moieties in the complexes, as confirmed by the XRD analysis (*vide supra*). On the basis of prior spectroscopic work with uranyl complexes of the Schiff-base type used here, the measured reductions can be assigned as $U^{VI}/U^{V}$ couples in both cases. And, as the anodic and cathodic waves are linearly proportional to the square root of scan rate, both the $U^{VI}$ and $U^{V}$ forms of $\mathbf{L^5UO_2}$ and $\mathbf{L^6UO_2}$ are soluble and freely diffusing as anticipated (see ESI, Fig. S80–S93†).[38]

Addition of one equivalent of the secondary cations ($Cs^+$, $Rb^+$, $K^+$, $Na^+$, $Li^+$, and $Ca^{2+}$) results in a shift of the $E_{1/2}$ value to a more positive potential. Across the series of complexes, the more positive shifts are associated with the more Lewis acidic cations, such that $Li^+$ engenders shifts in $E_{1/2}$ of +310 mV for $\mathbf{L^5UO_2Li}$ and +300 mV for $\mathbf{L^6UO_2Li}$, while $Ca^{2+}$ engenders shifts of +740 for $\mathbf{L^5UO_2Ca}$ and +650 mV for $\mathbf{L^6UO_2Li}$. In all

**Table 2** Electrochemical characteristics and $K_a$ (binding constant) values from NMR titration studies for the series of $\mathbf{L^5UO_2M}$ and $\mathbf{L^6UO_2M}$ complexes

| | $\mathbf{L^5UO_2M}$ | | | | | $\mathbf{L^6UO_2M}$ | | | | |
|---|---|---|---|---|---|---|---|---|---|---|
| **M** | $E_{1/2}$/mV *vs.* $Fc^{+/0}$ | $\Delta E_p$/mV | $k^0$/cm $s^{-1}$ (X $10^{-3}$) | $K_a/M^{-1}$ | $\Delta\delta_{max}{}^1H$ [a]/ppm | $E_{1/2}$/mV *vs.* $Fc^{+/0}$ | $\Delta E_p$/mV | $k^0$/cm $s^{-1}$ (X $10^{-3}$) | $K_a/M^{-1}$ | $\Delta\delta_{max}{}^1H$ [a]/ppm |
| None | −1.57 | 77 | 9.5 ± 4.0 | — | — | −1.53 | 74 | 14.6 ± 2.5 | — | — |
| $Cs^+$ | −1.40 | 108 | 3.4 ± 1.0 | 550 ± 80 | 0.04 | −1.38 | 113 | 5.7 ± 1.9 | $>10^5$ | 0.03 |
| $Rb^+$ | −1.40 | 100 | 4.9 ± 1.1 | 1370 ± 130 | 0.05 | −1.37 | 89 | 6.9 ± 1.4 | $>10^5$ | 0.04 |
| $K^+$ | −1.37 | 91 | 5.2 ± 1.8 | 1840 ± 260 | 0.07 | −1.36 | 83 | 14.3 ± 1.5 | $>10^5$ | 0.04 |
| $Na^+$ | −1.27 | 86 | 7.4 ± 1.3 | $>10^5$ | 0.11 | −1.35 | 79 | 13.5 ± 2.1 | $>10^5$ | 0.09 |
| $Li^+$ | −1.25 | 130 | 2.0 ± 0.3 | $>10^5$ | 0.12 | −1.23 | 185 | 0.9 ± 0.1 | 1370 ± 180 | 0.21 |
| $Ca^{2+}$ | −0.83 | 293 | 0.3 ± 0.1 | 9730 ± 5900 | 0.17 | −0.88 | 348 | 0.2 ± 0.1 | — | 0.15 |

[a] The uncertainty associated with measurements of $^1H$ NMR chemical shifts, $\delta^1H$, in our experiments is ±0.003 ppm (reported as ±1$\sigma$) based on replicate linewidth measurements. See ESI, Fig. S163 and Table S11 on p. 139.†


This journal is © The Royal Society of Chemistry 2025

Open Access Article. Published on 12 March 2025. Downloaded on 6/5/2026 2:38:04 PM.
This article is licensed under a Creative Commons Attribution-NonCommercial 3.0 Unported Licence.

cases, scan rate-dependent studies confirmed that the heterobimetallic species remain fully diffusional in both the U(v) and U(vi) oxidation states. Plotting all the measured $E_{1/2}$ values for the heterobimetallic species obtained with the monometallic cations in each ligand family as a function of the p$K_a$ values of the corresponding metal aqua complexes reveals linear correlations in both cases of −63 ± 10 and −49 ± 14 mV/p$K_a$, respectively (see Fig. 7). These values are indistinguishable within the uncertainty of the least-squares fitting used to determine the sensitivity of the relationship, and similar trend lines result from inclusion of the data for $Ca^{2+}$ and/or using the cathodic peak potentials ($E_{p,c}$) in place of the formal $E_{1/2}$ values (see ESI, Fig. S94–S96†). Consequently, we conclude that the cation-induced shift in solution redox chemistry is indistinguishable across the **$L^5UO_2M$** and **$L^6UO_2M$** series.

In order gain further insight into the cation-modulated electrochemical properties of the heterobimetallic species reported here, electrochemical titrations were carried out (see ESI, pp. S95–S110†). In this work, solutions containing **$L^6UO_2$** were titrated with a standard series of triflate salts (KOTf, NaOTf, LiOTf, and $Ca(OTf)_2$) in order to understand the interactions that may be occurring between the as-prepared U(vi) and electrogenerated formally U(v) forms of the complexes. Additionally, we were interested in understanding if flooding the system with excess metal cation in each case would lead to significant changes in the accessible redox chemistry. As direct cation-uranyl interactions could influence the heterogeneous electron transfer kinetics studied in this work, the nature of the binding of cations to the U(vi) and U(v) forms is particularly pertinent to this study and can be interrogated through these titrations as well.

The data corresponding to titration of **$L^6UO_2$** with KOTf confirm key features of the chemical behavior of the resulting **$L^6UO_2K$**. Generally speaking, binding of $K^+$ in the 18-crown-6-like site appears tight; there is a virtually isosbestic conversion of the starting monometallic complex to the expected bimetallic species up to addition of 1 equiv. of $K^+$ (see Fig. S97†). Importantly, over this range, there is not a gradual shift in the value of $E_{1/2}$ that would indicate rapid exchange on the electrochemical timescale. Instead, the redox wave for the parent monometallic complex diminishes cleanly and a new wave for **$L^6UO_2K$** grows in cleanly as the cation concentration increases. This suggests that $K^+$ binding to both the formal U(vi) and U(v) forms of the complex is fast and irreversible on the timescale explored here. Additionally, the redox waves for both the monometallic and bimetallic complexes compare well with the data shown in Fig. 6, suggesting that the presence of U:**M** ratios less or greater than 1 : 1 do not result in chemical reactivity beyond 1 : 1 cation binding (see Table S5†). Importantly, the presence of excess $K^+$ (up to 10 equiv.) does not contribute to changes in the appearance of the redox wave for the bimetallic species, suggesting little tendency of the uranyl oxo moieties in the electrogenerated, formally U(v) form to bind $K^+$ under these conditions. Similar profiles were measured in this data regardless of the number of cycles of voltammetry carried out, further underscoring the conclusion that $K^+$ does not

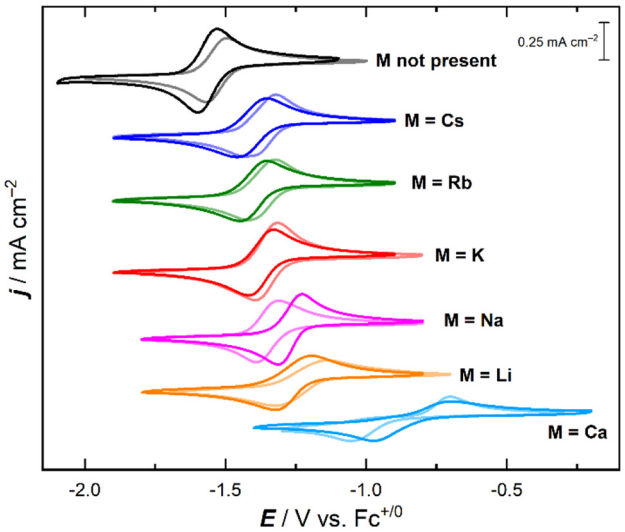


**Fig. 6** *In situ* cyclic voltammetry experiments for uranium complexes used in this study. **$L^5UO_2$** and **$L^5UO_2M$** complexes are represented by solid colors; **$L^6UO_2$** and **$L^6UO_2M$** complexes are represented by faded colors. Electrolyte: 0.1 M $TBAPF_6$ in $CH_3CN$, scan rate: 100 mV $s^{-1}$, electrode: highly oriented pyrolytic graphite.

interact strongly with either the U(vi) or U(v) forms of **$L^6UO_2$** beyond binding in the 18-crown-6-like site.

The results from titrations involving NaOTf (pp. S100–S102†), LiOTf (pp. S103–S106†), and CaOTf (pp. S107–S110†) are similar, suggesting tight and irreversible binding of 1 equiv. of **M** to the starting **$L^6UO_2$** in each case. Additions of each cation beyond 1 equiv. were not associated with significant changes in the electrochemical profiles measured, apart from the anticipated dilution of the uranium-containing solution that led to diminished reductive and oxidative peak currents ($i_{p,c}$ and $i_{p,a}$ values) in the voltammograms associated with the solutions containing the greatest cation concentrations. Consequently, we conclude that all of the tested cations interact strongly with both U(vi) and U(v) by binding in the 18-crown-6-like site.

As formation of insoluble oxo-bridged multimetallic uranium species is a recognized reactivity mode of U(v) complexes, we particularly searched for evidence of formation of such species in the titration studies reported here. No significant electrode fouling was encountered in any case as confirmed by appropriate wipe tests (see Fig. S104 and S108†) and multicycling experiments (Fig. S98, S101, S105, and S109†). A very minor feature that appears to be associated with electrode modification was observable after significant numbers of cycling experiments, but as this feature was not found to vary significant with cation identity (Fig. S112 and S113†), we do not anticipate that it is associated with a soluble, molecular uranium-containing species. Consequently, based on the overall results from the titration studies, there is virtually no evidence of formation of oxo-bridged heterobimetallic species in solution either in the U(vi) or U(v) oxidation states. This conclusion is in accord with Raman studies carried out on the

Open Access Article. Published on 12 March 2025. Downloaded on 6/5/2026 2:38:04 PM.
This article is licensed under a Creative Commons Attribution-NonCommercial 3.0 Unported Licence.

1 : 1 U : **M** species in solution (*vide infra*) and with the general finding that the U(VI)/U(V) reduction potential does not depend on the added cation concentration beyond 1 equiv. (see Fig. S111†). And, all this suggests that the formation of oxo-bridged species is not likely to drive the measured changes in heterogeneous electron transfer rates as a function of cation (**M**) identity, since the availability of free cation in solution (not bound in the 18-crown-6-like site) could be anticipated to encourage formation of such species more readily than when the only cation available for formation of oxo-bridged species is already bound in the 18-crown-6-like site.

### Raman spectroscopic interrogation of the uranyl moieties

We anticipated that a more detailed examination of the properties of the uranyl moiety in each heterobimetallic complex should be pursued. This is because the shift in $U^{VI}/U^{V}$ reduction potential measured for both families of complexes is attributable to the electrostatic influence of the secondary cations on the uranyl moiety in both the U(VI) and U(V) oxidation states. Considering this, it would be virtually impossible to reliably attribute changes in the reduction potential to structural or electrostatic considerations known only for the oxidized form of the complexes, because the bound cations should influence the properties of both the U(VI) and U(V) forms. We anticipated, however, that it would be quite feasible to measure the dependence of vibrational features of the uranyl system in each ligand as a function of the incorporated secondary metal cation. With this approach, we anticipated that we could cross-correlate cation-dependent properties for the isolated complexes available to us in the U(VI) oxidation state. In this case, Raman spectroscopy appealed to us immediately as this technique has been firmly established as a useful probe of the uranium-oxo symmetric stretching mode (commonly denoted $\nu_1$ or $\nu_{sym}$ in the literature). From the Raman data, we envisioned that we might measure modulation of the donor power of the bridging phenoxide ligands to the uranyl motif induced by incorporation of the secondary metal cations to the complexes **L$^5$UO$_2$M** and **L$^6$UO$_2$M**.

Raman spectra were thus collected on crystalline samples of the heterobimetallic complexes.‖ Derivatives in the **L$^5$UO$_2$M** series where **M** = $Rb^+$, $K^+$, $Na^+$, $Li^+$, and $Sr^{2+}$ were investigated, while work with the **L$^6$UO$_2$M** system was conducted with **M** = $Rb^+$, $K^+$, $Na^+$, $Sr^{2+}$, $Ca^{2+}$, and $La^{3+}$. Spectra were also collected on crystalline samples of **L$^5$UO$_2$** and **L$^6$UO$_2$**. In the case of **L$^5$UO$_2$** and **L$^6$UO$_2$**, $\nu_{sym}$ appeared at 812 and 813 $cm^{-1}$, respectively (see ESI, Fig. S39, S46, and Tables S1, S2†). For the heterobimetallic **L$^5$UO$_2$M** and **L$^6$UO$_2$M** complexes, $\nu_{sym}$ frequencies for the U–$O_{oxo}$ units were measured across the range of 812–819 $cm^{-1}$ for the **L$^5$UO$_2$M** complexes and across a wider range from 807–828 $cm^{-1}$ for the **L$^6$UO$_2$M** complexes (see ESI, Tables S1 and S2†). The similar $\nu_{sym}$ values for the monometallic complexes can be attributed to the similar uranium coordination environments in both cases, as confirmed by the XRD analysis. Incorporation of secondary metal cations into either **L$^5$UO$_2$** or **L$^6$UO$_2$** generally resulted in either no significant shift (including minor red-shifts) of the $\nu_{sym}$ or a more substantial blue shift; the shift measured appears to depend on the identity and characteristics of the particular incorporated cation (see ESI, pp. S34–S63†). Blue shifting, in this context, can be interpreted as being indicative of a relative strengthening of the U–$O_{oxo}$ bonding upon formation of the heterobimetallic species. This phenomenon can be attributed to a charge density effect induced by interaction of the secondary metal cations with the phenoxide ligands that bridge to the uranium center. Of course, metal cations that are less charge dense would be anticipated to afford little to no blue shift in the measured value of $\nu_{sym}$, owing to the meager power of those particular cations to modulate the donor power of the bridging phenoxide moieties to the uranium center.[13]

Plotting the symmetric stretching frequencies for each series of the heterobimetallic complexes as a function of the

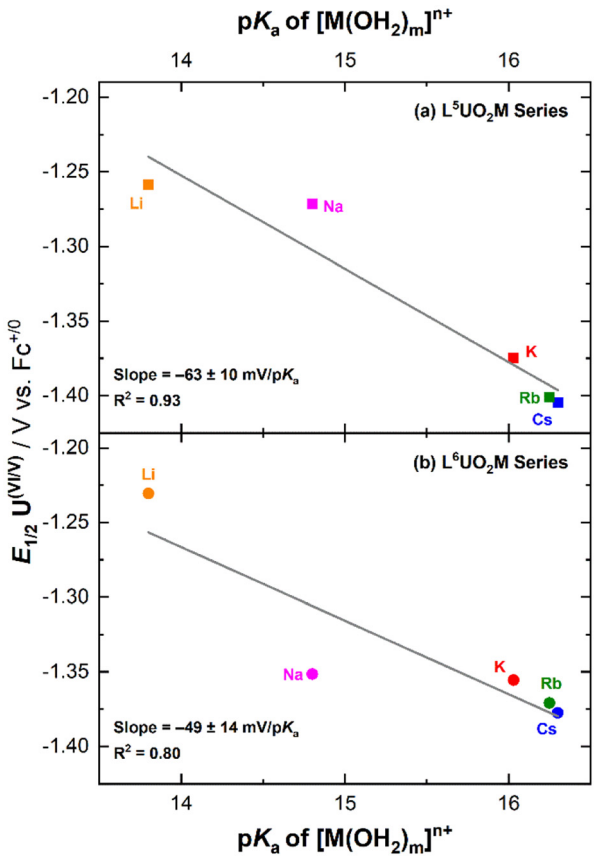


**Fig. 7** Plot of $E_{1/2}(U^{VI/V})$ *vs.* p$K_a$ of $[M(H_2O)_m]^{n+}$ for **L$^5$UO$_2$M** complexes (a, upper panel) and **L$^6$UO$_2$M** complexes (b, lower panel).

‖ IR spectra for the **L$^6$UO$_2$M** series were also collected, revealing features from 884 to 893 $cm^{-1}$ (Fig. S66–S72†) that could be associated with asymmetric U–$O_{oxo}$ stretching. However, there is no systematic trend in the data, suggesting that intra-ligand vibrations could cloud identification of U–$O_{oxo}$ stretching. Similarly, IR spectra were collected in the far, low-energy region, revealing similar features in all cases from 252 to 256 $cm^{-1}$ (Fig. S73–S79†) that could be associated with U–$O_{oxo}$ bending modes,[47] but no trend in the measured frequencies was identified.


This journal is © The Royal Society of Chemistry 2025

Open Access Article. Published on 12 March 2025. Downloaded on 6/5/2026 2:38:04 PM. This article is licensed under a Creative Commons Attribution-NonCommercial 3.0 Unported Licence.

$pK_a$ values of the corresponding metal aqua complexes revealed a linear relationship for both the $\mathbf{L^5UO_2M}$ and $\mathbf{L^6UO_2M}$ series (Fig. 8). The trend line in the data for the $\mathbf{L^5UO_2M}$ series has a shallower dependence of −1.21 ± 0.51 $cm^{-1}/pK_a$ than that measured for the $\mathbf{L^6UO_2M}$ series at −4.21 ± 0.70 $cm^{-1}/pK_a$, when comparing the data available for the mono- and divalent cations. (The result is similar when including data for $\mathbf{L^6UO_2La}$ as well; see ESI, Fig. S54.†) The substantial difference in the slopes of the trend lines (greater than their combined uncertainties) can be readily attributed to the distinguishing feature of the two series of complexes that was observed in the XRD analysis; namely, in the solid state, the secondary cations are bound well above the macrocyclic plane in the $\mathbf{L^5UO_2M}$ series, whereas in the $\mathbf{L^6UO_2M}$ series, the metal cations are effectively encapsulated by the 18-crown-6-like site. This conclusion, quantified based on the tabulated $\psi_M$ parameters for the complexes, is notable when compared to findings in a recent analysis of the influence of secondary cations on the asymmetric stretching frequency of the vanadyl ion, $[VO]^{2+}$, measured with infrared spectroscopy.[13] In both cases, there is an apparent linear relationship between the tendency for the secondary metal cations to diminish the donor ability of the bridging phenoxides to the uranium center, driving the generally blue-shifted vibrational characteristics in both cases. These spectroscopic shifts depend only on the structures of the U(VI) forms of the complexes, in contrast to the electrochemical work in which U(V) forms also must be considered. This is noted as a key difference between the spectroscopic and electrochemical work reported here (Table 3).

Along this line, the solid-state Raman spectrum collected for crystalline $\mathbf{L^6UO_2Li}$ revealed $\nu_{sym}$ at 811 $cm^{-1}$. This value does not align with the trend line measured for the other heterobimetallic complexes, a finding attributable to the dimeric nature of the complex in the solid state as observed by XRD. We anticipate that the direct U–$O_{oxo}$···Li interactions causes this deviation, a notion supported by observation of a distinctive signal for $\mathbf{L^6UO_2Li}$ at 897 $cm^{-1}$ (see ESI, Fig. S50†) that is absent in the spectra of other complexes studied. The feature at 897 $cm^{-1}$ can be assigned as the asymmetric stretching mode (commonly denoted $\nu_3$ or $\nu_{as}$), observable under these conditions due to lowered site symmetry of the $[UO_2]$ motif upon direct interaction with $Li^+$. The $\nu_{as}$ feature for $\mathbf{L^6UO_2Li}$ was also observed by infrared spectroscopy at a similar estimated energy of 892 $cm^{-1}$ (see p. S67†). However, in line with the clean electrochemical behavior observed by cyclic voltammetry, a Raman spectrum collected on a solution of the $\mathbf{L^6UO_2Li}$ complex revealed a feature that corresponds to $\nu_{sym}$ at 821 $cm^{-1}$ (see ESI, Fig. S59†) This frequency compares well with the $\nu_{sym}$ values of the other complexes in the $\mathbf{L^6UO_2M}$ family in solution (Table S3†), indicating that the cations remain bound in solution but that the dimeric form of $\mathbf{L^6UO_2Li}$ can be readily cleaved into individual heterobimetallic species in solution. To further interrogate the possibility of dimerization of $\mathbf{L^6UO_2Li}$ in solution, we collected Raman spectra in $CH_3CN$ solution across a range of concentrations from 1–25 mM (see ESI, pp. S62–S63†). There was no significant change in the established $\nu_{sym}$ value of 821 $cm^{-1}$ for the compound across this range, suggesting that dimerization and/or other speciation of this system does not occur under these conditions. We anticipate that these observations are all consistent with the coordinating nature of $CH_3CN$, which

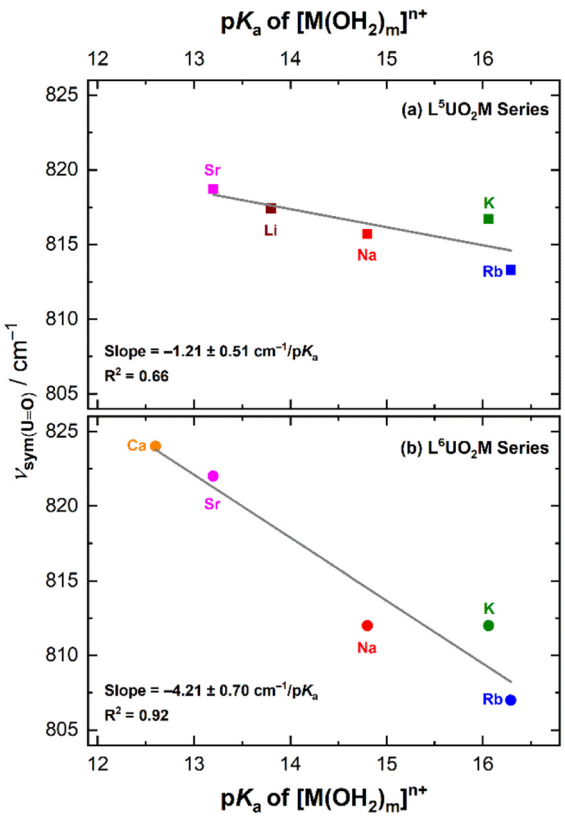


**Fig. 8** Dependence of the U=O symmetric stretching frequency from Raman spectroscopy of the $\mathbf{L^5UO_2M}$ (a, upper panel) and $\mathbf{L^6UO_2M}$ (b, lower panel) complexes on the Lewis acidity ($pK_a$) of the corresponding metal cation aqua complexes.

**Table 3** $\nu_{sym}$ stretching frequencies from solid-state Raman spectroscopy for the $\mathbf{L^5UO_2M}$ and $\mathbf{L^6UO_2M}$ series of complexes

| Series of complexes | M | $pK_a$ of $[M(H_2O)_m]^{n+}$ | $\nu_{sym}$ |
|---|---|---|---|
| $\mathbf{L^5UO_2M}$ | $Rb^+$ | 16.29[a] | 813 |
| | $K^+$ | 16.06[a] | 817 |
| | $Na^+$ | 14.8[b] | 816 |
| | $Li^+$ | 13.8[b] | 817 |
| | $Sr^{2+}$ | 13.2[b] | 819 |
| $\mathbf{L^6UO_2M}$ | $Rb^+$ | 16.29[a] | 807 |
| | $K^+$ | 16.06[a] | 811 |
| | $Na^+$ | 14.8[b] | 811 |
| | $Li^+$ | 13.8[b] | 811 |
| | $Sr^{2+}$ | 13.2[b] | 822 |
| | $Ca^{2+}$ | 12.6[b] | 824 |
| | $La^{3+}$ | 9.1[b] | 828 |

[a] From ref. 39. [b] From ref. 40.

Open Access Article. Published on 12 March 2025. Downloaded on 6/5/2026 2:38:04 PM.
This article is licensed under a Creative Commons Attribution-NonCommercial 3.0 Unported Licence.

appears suitable for breaking apart the dimeric species observed in the solid-state XRD data.

In accord with all these observations, a tight linear correlation of −1.64 ± 0.31 $cm^{-1}/pK_a$ between $\nu_{sym}$ and the $pK_a$ of $[M(OH_2)_m]^{n+}$ was observed upon comparing all the solution-phase spectra (Fig. S63†), confirming that the cations' influence over the properties of the uranyl system are persistent in solution. At this stage, we have not assigned an interpretation to the magnitudes of the correlations for the **$L^6UO_2M$** series in the solution *vs.* in the solid state, although we anticipate that the difference is attributable to solvation of the complexes upon dissolution.

### Heterogeneous electron transfer kinetics

The trends measured among the reduction potentials and symmetric O–U–O stretching modes for the heterobimetallic complexes confirm that incorporation of the secondary metal cations results in more electron-poor uranium centers. This change in charge density is reflected in both the increased energies for the O–U–O stretching modes and the more positive reduction potentials. However, inspection of the electrochemical data revealed another set of cation-dependent behaviors. Namely, there is a distinct change in the peak-to-peak separations ($\Delta E_p$) of the redox waves across each series of complexes. As shown in Table 2, the $\Delta E_p$ values for the **$L^5UO_2M$** complexes increase (at 100 mV $s^{-1}$) going from the derivatives incorporating $Cs^+$, $Rb^+$, $K^+$, and $Na^+$, but then decrease again from $Na^+$ to $Li^+$ to $Ca^{2+}$ (see Table 2). The results for the **$L^6UO_2M$** series are similarly non-monotonic, but in the case of that series of complexes, as the $\Delta E_p$ values are similar for $Na^+$ and $K^+$ and for $Li^+$ and $Ca^{2+}$. Observing this, we initially imagined that the Lewis acidity (or another property) of the incorporated secondary metal cation, the cation's binding affinity, and/or geometric rearrangements on reduction could drive these changes in $\Delta E_p$.

In order to examine this trend in a quantitative fashion, we determined the standard heterogeneous electron transfer rate constant, denoted $k^0$, for each complex using the traditional method of Nicholson.[41] In our method (see ESI, p. S140† for details), we measured the $\Delta E_p$ values for the complexes in each series at six different scan rates, and then determined an average $k^0$ value (given in Table 2). As expected, there was little variability in the measured $k^0$ values across scan rates; this is reflected in the low uncertainty associated with the average $k^0$ values and is indicative of $k^0$ being invariant with scan rate as expected from electrochemical theory.[42]

Plotting the $k^0$ values for each series of complexes as a function of the Lewis acidity of the incorporated secondary metal cation revealed "volcano plots" in each case (see Fig. 9). As expected on the basis of the $\Delta E_p$ values, the complexes containing the most Lewis acidic cations in our series, $Li^+$ and $Ca^{2+}$, display the slowest electron transfer kinetics (reflected in small $k^0$ values). In the **$L^5UO_2M$** series, **$L^5UO_2Na$** displays the fastest electron transfer kinetics, whereas in the **$L^6UO_2M$** series, both **$L^6UO_2Na$** and **$L^6UO_2K$** display fast kinetics that are indistinguishable within the uncertainty of our measurements. These findings suggest that the interplay of factors mentioned

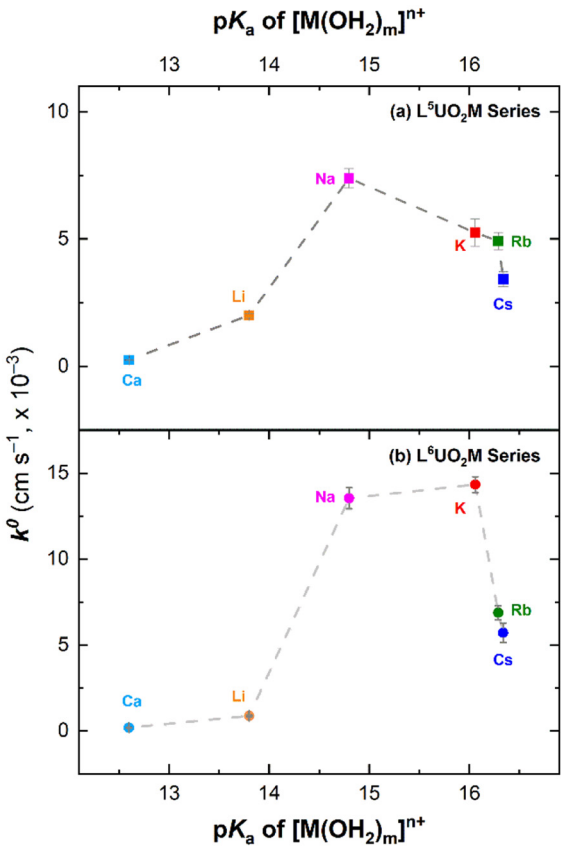


Fig. 9 Plots of $k_0$ *vs.* $pK_a$ of $[M(H_2O)_m]^{n+}$ for **$L^5UO_2M$** complexes (a, upper panel) and **$L^6UO_2M$** complexes (b, lower panel).

above could govern the electrochemical reversibility of the $U^{VI}/U^V$ reduction manifold. Lewis acidity does appear to be an influence, a finding attributable to the tendency of a strongly Lewis acidic cations to engender chemical reactivity. However, on the basis of the titration experiments, chemical reorganization of the complexes upon generation of U(v) involving direct interaction of the secondary metal cations with the oxo ligands of the uranyl system upon reduction is unlikely.

Tight binding of the cations in the crown-ether-like sites of **$L^5UO_2$** and **$L^6UO_2$** would likely improve electrochemical reversibility by minimizing reorganization before/after reduction. Along this line, the diminished electron transfer kinetics associated with the derivatives of both **$L^5UO_2$** and **$L^6UO_2$** incorporating $Rb^+$ and $Cs^+$ are suggestive of a poor size match, and thus weaker binding, of these cations for/in the 15-crown-5- and 18-crown-6-like sites. As result, the cations are likely more easily lost from the crown sites, particularly upon uranium-centered reduction. We were unable to grow diffraction-quality crystals of the $Rb^+$ and $Cs^+$ complexes despite many attempts, a finding in accord the poor size match of these cations with the crown sites in the complexes.

### Quantification of cation binding strength

To provide data for interpreting the cation influence over the electron transfer kinetics, we measured the binding constants


This journal is © The Royal Society of Chemistry 2025

Open Access Article. Published on 12 March 2025. Downloaded on 6/5/2026 2:38:04 PM.
This article is licensed under a Creative Commons Attribution-NonCommercial 3.0 Unported Licence.

($K_a$ values) of the cations in the monometallic complexes in $CD_3CN$. The $K_a$ values were measured with titrations relying on $^1H$ nuclear magnetic resonance (NMR) spectroscopy; in our method, the chemical shift value ($\delta^1H$) associated with the three equivalent protons of the methyl group of each complex was found to be correlated in each case with increasing concentrations of the triflate salts of the individual cations. The change in the $\delta^1H$ value ($\Delta\delta^1H$) was thus used to determine the value of $K_a$ by fitting to the 1 : 1 binding isotherm.[43] As discussed in prior work on use of titrations with phosphine-oxide probes to study cation behaviors, satisfactory fits to this isotherm provide support for 1 : 1 binding stoichiometry.[39] The titration data also provide a readout of the maximum achievable change in chemical shift ($\Delta\delta_{max}{}^1H$) as well, representing detailed information of the influence of the given secondary metal cation on the heterobimetallic species that is independent of its binding constant ($K_a$ value). Stated another way, the $\Delta\delta_{max}{}^1H$ values describe the maximum possible de-shielding of the methyl protons, specifically at the condition where the metal ion of interest is maximally occupying its binding site.

In each set of titration data, the $\Delta\delta^1H$ value initially undergoes significant changes at lower titrant cation equivalencies but eventually levels off at higher equivalencies (see ESI, pp. S114–S137†). The plateauing behavior is indicative of clean binding of 1 equiv. of cation in the crown-like-site in each case, even when large excesses (>5 equiv.) of the metal cations were added. For some cases, very tight binding was implied in the data, and for these cases, fitting to the 1 : 1 binding isotherm was not possible; the data in these cases suggest only a lower estimate of the $K_a$ value.

The $K_a$ values for binding of $Cs^+$, $Rb^+$, $K^+$, and $Na^+$ in the crown site of $\mathbf{L^5UO_2}$ increase in the same order, a trend that is in agreement with the ionic radii of these cations. Similar to findings for related, purely organic 15-crown-5 derivatives, the $Na^+$ ion binds tightly to $\mathbf{L^5UO_2}$.[44] $Li^+$ also binds quite tightly to $\mathbf{L^5UO_2}$, a finding in accord with the results of XRD analysis for $\mathbf{L^5UO_2Li}$ that confirmed the ability of the 15-crown-5-like site in this case to bind $Li^+$. For $Ca^{2+}$, titration results indicate more modest binding; the weaker binding in comparison to $Na^+$ and $Li^+$ could be attributable to the steric bulk associated with the two triflate counteranions accompanying $Ca^{2+}$, as in the XRD structure, both triflates are restricted to binding to $Ca^{2+}$ on the same hemisphere or face of the overall heterobimetallic species.

Tight associations of $Cs^+$, $Rb^+$, $K^+$, and $Na^+$ with $\mathbf{L^6UO_2}$ were measured in all cases, in accord with the larger size the 18-crown-6-like site in comparison to the 15-crown-5-like site in $\mathbf{L^5UO_2}$. However, the binding of these cations is sufficiently strong to preclude detailed comparisons among them (Table 2 and Fig. S162†). Such large binding coefficients (>$10^5$ $M^{-1}$) are sensible, however, given the recognized ability of 18-crown-6 species to bind a variety of metal cations.

We also examined the $\Delta\delta_{max}{}^1H$ values from the titrations for any trends. Plotting the $\Delta\delta_{max}{}^1H$ values as a function of the p$K_a$ values resulted in reasonable linear correlations in both cases (Fig. 10). These data show that the more acidic cations result in more significant charge-density-driven perturbations in the heterobimetallic complexes. The observation of reasonable linear correlations in the NMR titration data and values of $\Delta\delta_{max}{}^1H$ for both the $\mathbf{L^5UO_2M}$ and $\mathbf{L^6UO_2M}$ series of complexes is commensurate with the other linear trends measured in this work.

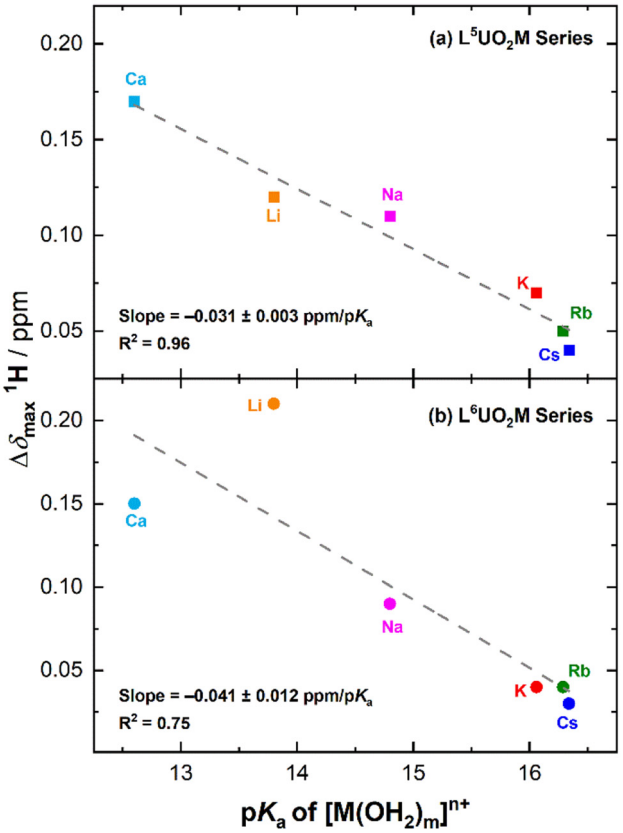


**Fig. 10** Plots of $\Delta\delta_{max}{}^1H$ *vs.* p$K_a$ of $[M(H_2O)_m]^{n+}$ for $\mathbf{L^5UO_2M}$ complexes (a, upper panel) and $\mathbf{L^6UO_2M}$ complexes (b, lower panel).

## Discussion

The heterogeneous electron transfer rate constants for both the $\mathbf{L^5UO_2M}$ and $\mathbf{L^6UO_2M}$ series of complexes appear to be influenced by both the association constants for cation binding and the Lewis acidities of the cations. For $\mathbf{L^5UO_2M}$, the smaller 15-crown-5 like site engenders behavior in which only $Na^+$ and $Li^+$ are bound very tightly. This result is in agreement with observation of the fastest ET kinetics for $\mathbf{L^5UO_2Na}$. $Li^+$ and $Ca^{2+}$ are more Lewis acidic cations, but the origin of the diminished $k^0$ values for these cations is not yet clear; reactivity with nascent uranium(v) species is not supported by related electrochemical titration data. However, the binding of $Na^+$ is significantly stronger than that of $Li^+$ in the polyether site; comparing to the organic crown literature, our system follows the natural preference of 15-crown-5-type species for binding of $Na^+$.[23,45] This could suggest that the lithium system

Open Access Article. Published on 12 March 2025. Downloaded on 6/5/2026 2:38:04 PM.
This article is licensed under a Creative Commons Attribution-NonCommercial 3.0 Unported Licence.

undergoes greater reorganization after reduction, perhaps involving displacement of the bound triflate counteranion.

For the heterobimetallic species in the $\mathbf{L^6UO_2M}$ family, similar results were obtained, but with a shift in the trends that is correlated with tightest binding of both $Na^+$ and $K^+$. Our data do not distinguish between these cations in terms of binding strength, but the fast electron transfer kinetics in both cases is consistent with the tight binding of these ions. As in the $\mathbf{L^5UO_2M}$ series, use of the more Lewis acidic cations $Li^+$ or $Ca^{2+}$ or the anticipated weaker binding $Cs^+$ or $Rb^+$ was found to be associated with slower electron transfer kinetics, but the precise mechanisms underpinning this behavior is not yet clear. Reorganization penalties associated with displacement of bound triflate, or other ligands, are possible in the $\mathbf{L^6UO_2M}$ series as in $\mathbf{L^5UO_2M}$.

This study has generated a set of electrochemical and spectroscopic data suitable for quantitatively interpreting the rational influence that secondary metal cations exert over the uranyl moiety in heterobimetallic complexes. The p$K_a$-dependence of the $U^{VI}/U^{V}$ reduction potentials measured by cyclic voltammetry and the uranyl symmetric stretching vibrations measured by Raman spectroscopy suggest that the U(VI) centers in the heterobimetallic complexes become more electron deficient upon incorporation of secondary metal cations. A quantitative dependence on Lewis acidity of this type (involving vibrational spectroscopic and electrochemical evidence) has not been reported previously, to the best of our knowledge. However, this finding is reminiscent of recent work from Blakemore and co-workers[13] that examined the use of a crown-containing ligand for the vanadyl dication, $[VO]^{2+}$, as a spectroscopically and electrochemically addressable probe molecule in a set of heterobimetallic complexes; evidence was assembled in support of the hypothesis that the influence of secondary cations could be understood to arise from modulation of the donor strength of phenoxide ligands that bridged to the vanadium center. Here, Raman spectroscopy was used to probe the more symmetrical *trans*-dioxo uranyl system, and results in accord with cation-driven changes in bridging ligand donor power were obtained.

The secondary cations in the heterobimetallic complexes studied here appear to modulate the donor strength of the phenoxide moieties that interact with both the secondary cation and the uranium center in each species. Use of p$K_a$ values as the descriptor for Lewis acidity is sensible given the ability for secondary cations to polarize bound water molecules, resulting in the unique p$K_a$ value for each metal cation.[46] The robust trends shown in Fig. 7 and 8 show that the p$K_a$ values can be used, similarly, to describe the polarization the phenoxide moieties in the heterobimetallic complexes studied here. Any other effects wrought by the incorporated cations appear subordinate to this first coordination-sphere effect.

In light of the consistent trends in the electrochemical and spectroscopic data presented in this manuscript, use of tailored macrocyclic ligand systems in concert with Lewis acidic metal cations can be concluded to be a useful strategy for controlling the redox properties of the uranyl dication. In the systems studied here, the ligand systems $\mathbf{H_2L^5}$ and $\mathbf{H_2L^6}$ enable formation of heterobimetallic species that would, most likely, not otherwise form in solution or persist for chemical investigations. Future work could focus on structural and spectroscopic investigations of the formally U(V) forms of the complexes, building on the useful features encountered during study of the U(VI) forms reported here. We anticipate that detailed study of the U(V) species would provide an even richer platform upon which to study cation-modulated actinide redox chemistry, considering the greater reactivity of U(V) in comparison to U(VI). Investigations along this line are currently underway in our laboratories.

## Conclusions

Here, structural changes to supporting macrocyclic ligands have been shown to tune the ability of secondary metal cations to influence the electronic properties of the uranyl dication, $UO_2^{2+}$. The association constants of the secondary cations with the parent uranyl-containing species were tuned by the ligand design, giving a structural handle for harnessing cations' inherent Lewis acidity properties. Raman spectroscopy and electrochemistry have been used to demonstrate quantitative relationships between cation Lewis acidity and diminished bridging-ligand donation to uranium, affording a spectroscopic counterpart to the measured redox. Taken together, these studies demonstrate the broad usefulness of Lewis acidity as a descriptor for the properties of multimetallic actinide complexes, and suggest further opportunities for ligand design to impact studies of multimetallic actinide chemistry.

## Conflicts of interest

There are no conflicts to declare.

## Acknowledgements

The authors thank Dr Justin Douglas and Sarah Neuenswander for assistance with NMR spectroscopy, and Michael Lemon and Alice Dale for assistance with radiation safety protocols. This work was supported by the U.S. Department of Energy, Office of Science, Office of Basic Energy Sciences through the Early Career Research Program (DE-SC0019169). The authors also acknowledge the US National Institutes of Health for support of the NMR instrumentation (S10OD016360 and S10RR024664) used in this study. T. Z. F. and M. K. P. acknowledge U.S. Department of Energy, Office of Science, Office of Basic Energy Sciences through the Heavy Element Chemistry Program (DE-SC0021420) for the spectroscopic experiments that were performed at the University of Iowa. K. P. C. was supported by start-up funding from the College of Liberal Arts and Sciences and the Department of Chemistry at the University of Iowa.


This journal is © The Royal Society of Chemistry 2025

Open Access Article. Published on 12 March 2025. Downloaded on 6/5/2026 2:38:04 PM. This article is licensed under a Creative Commons Attribution-NonCommercial 3.0 Unported Licence.

Solid-state mid- and far-IR spectra were collected on an instrument funded by a Nuclear Regulatory Commission Faculty Development Grant (NRC 31310018M0042).

## References

1 B. M. T. Costa Peluzo and E. Kraka, Uranium: The nuclear fuel cycle and beyond, *Int. J. Mol. Sci.*, 2022, **23**, 4655.
2 J. D. Navratil and W. W. Schulz, *Actinide Separations*, American Chemical Society, 1980, vol. 117.
3 (*a*) J. B. Starks, *Purex process*, DPSPU-77-11-1, TRN: 78-007289, United States, 1977; (*b*) J. M. Mckibben, Chemistty of the Purex Process, *Radiochim. Acta*, 1984, **36**, 3–16; (*c*) H. A. C. McKay, *The PUREX process*, CRC Press Inc., United States, 1990.
4 (*a*) M. F. Simpson and A. M. Casella, in *Engineering Separations Unit Operations for Nuclear Processing*, CRC Press, 2019, pp. 305–321; (*b*) M. J. Martínez-Rodríguez, L. C. Olson, J. R. Gray and B. L. García-Díaz, Non-Aqueous Electrochemical Fluorination of Used Nuclear Fuel as an Advanced Separation Process, *J. Electrochem. Soc.*, 2019, **166**, E231.
5 D. LeBlanc, Molten salt reactors: A new beginning for an old idea, *Nucl. Eng. Des.*, 2010, **240**, 1644–1656.
6 (*a*) R. G. Denning, Electronic structure and bonding in actinyl ions, *Complexes, Clusters and Crystal Chemistry*, 1992, pp. 215–276; (*b*) R. G. Denning, Electronic Structure and Bonding in Actinyl Ions and their Analogs, *J. Phys. Chem. A*, 2007, **111**, 4125–4143.
7 A. Bard, R. Parsons and J. Jordan, *Standard Potentials in Aqueous Solution*, M Dekker, New York, 1985.
8 J. W. Freiderich, E. Wanigasekara, X.-G. Sun, R. A. Meisner, H. M. Meyer, H. Luo, L. H. Delmau, S. Dai and B. A. Moyer, Direct Electrodeposition of $UO_2$ from Uranyl Bis(trifluoromethanesulfonyl)imide Dissolved in 1-Ethyl-3-methylimidazolium Bis(trifluoromethanesulfonyl)imide Room Temperature Ionic Liquid System, *Electrochim. Acta*, 2014, **115**, 630–638.
9 (*a*) S. Fukuzumi, Electron-transfer properties of high-valent metal-oxo complexes, *Coord. Chem. Rev.*, 2013, **257**, 1564–1575; (*b*) W. Nam, Y.-M. Lee and S. Fukuzumi, Tuning reactivity and mechanism in oxidation reactions by mononuclear nonheme iron(IV)-oxo complexes, *Acc. Chem. Res.*, 2014, **47**, 1146–1154; (*c*) S. Fukuzumi, K. Ohkubo, Y. M. Lee and W. Nam, Lewis acid coupled electron transfer of metal–oxygen intermediates, *Chem. – Eur. J.*, 2015, **21**, 17548–17559; (*d*) J. Park, Y. Morimoto, Y.-M. Lee, W. Nam and S. Fukuzumi, Unified view of oxidative C–H Bond cleavage and sulfoxidation by a nonheme Iron(IV)–Oxo complex via lewis acid-promoted electron transfer, *Inorg. Chem.*, 2014, **53**, 3618–3628.
10 A. Kumar, D. Lionetti, V. W. Day and J. D. Blakemore, Redox-inactive metal cations modulate the reduction potential of the uranyl ion in macrocyclic complexes, *J. Am. Chem. Soc.*, 2020, **142**, 3032–3041.
11 A. Kumar, D. Lionetti, V. W. Day and J. D. Blakemore, Trivalent Lewis acidic cations govern the electronic properties and stability of heterobimetallic complexes of nickel, *Chem. – Eur. J.*, 2018, **24**, 141–149.
12 R. R. Golwankar, A. Kumar, V. W. Day and J. D. Blakemore, Revealing the Influence of Diverse Secondary Metal Cations on Redox–Active Palladium Complexes, *Chem. – Eur. J.*, 2022, **28**, e202200344.
13 C. M. Dopp, R. R. Golwankar, S. R. Kelsey, J. T. Douglas, A. N. Erickson, A. G. Oliver, C. S. Day, V. W. Day and J. D. Blakemore, Vanadyl as a Spectroscopic Probe of Tunable Ligand Donor Strength in Bimetallic Complexes, *Inorg. Chem.*, 2023, **62**, 9827–9843.
14 J. P. Karnes, A. Kumar, J. A. Hopkins Leseberg, V. W. Day and J. D. Blakemore, Trivalent Cations Slow Electron Transfer to Macrocyclic Heterobimetallic Complexes, *Inorg. Chem.*, 2024, **63**, 8710–8729.
15 (*a*) J. S. Kanady, E. Y. Tsui, M. W. Day and T. Agapie, A synthetic model of the $Mn_3Ca$ subsite of the oxygen-evolving complex in photosystem II, *Science*, 2011, **333**, 733–736; (*b*) E. Y. Tsui, J. S. Kanady and T. Agapie, Synthetic Cluster Models of Biological and Heterogeneous Manganese Catalysts for $O_2$ Evolution, *Inorg. Chem.*, 2013, **52**, 13833–13848; (*c*) E. Y. Tsui, R. Tran, J. Yano and T. Agapie, Redox-inactive metals modulate the reduction potential in heterometallic manganese–oxido clusters, *Nat. Chem.*, 2013, **5**, 293–299; (*d*) D. Lionetti, S. Suseno, E. Y. Tsui, L. Lu, T. A. Stich, K. M. Carsch, R. J. Nielsen, W. A. Goddard III, R. D. Britt and T. Agapie, Effects of Lewis acidic metal ions (M) on oxygen-atom transfer reactivity of heterometallic $Mn_3MO_4$ cubane and $Fe_3MO(OH)$ and $Mn_3MO(OH)$ clusters, *Inorg. Chem.*, 2019, **58**, 2336–2345.
16 (*a*) A. H. Reath, J. W. Ziller, C. Tsay, A. J. Ryan and J. Y. Yang, Redox Potential and Electronic Structure Effects of Proximal Nonredox Active Cations in Cobalt Schiff Base Complexes, *Inorg. Chem.*, 2017, **56**, 3713–3718; (*b*) S. Maity, S. Ghosh and A. Ghosh, Elucidating the secondary effect in the Lewis acid mediated anodic shift of electrochemical oxidation of a Cu(II) complex with a $N_0O_2$ donor unsymmetrical ligand, *Dalton Trans.*, 2019, **48**, 14898–14913; (*c*) T. K. Ghosh, S. Maity, S. Ghosh, R. M. Gomila, A. Frontera and A. Ghosh, Role of Redox-Inactive Metal Ions in Modulating the Reduction Potential of Uranyl Schiff Base Complexes: Detailed Experimental and Theoretical Studies, *Inorg. Chem.*, 2022, **61**, 7130–7142.
17 (*a*) P. L. Arnold, D. Patel, C. Wilson and J. B. Love, Reduction and selective oxo group silylation of the uranyl dication, *Nature*, 2008, **451**, 315–317; (*b*) B. E. Cowie, J. M. Purkis, J. Austin, J. B. Love and P. L. Arnold, Thermal and photochemical reduction and functionalization chemistry of the uranyl dication, $[UVIO_2]^{2+}$, *Chem. Rev.*, 2019, **119**, 10595–10637.
18 (*a*) R. Faizova, S. White, R. Scopelliti and M. Mazzanti, The effect of iron binding on uranyl(v) stability, *Chem. Sci.*, 2018, **9**, 7520–7527; (*b*) V. Mougel, P. Horeglad, G. Nocton, J. Pécaut and M. Mazzanti, Cation–cation complexes of

Open Access Article. Published on 12 March 2025. Downloaded on 6/5/2026 2:38:04 PM. This article is licensed under a Creative Commons Attribution-NonCommercial 3.0 Unported Licence.

pentavalent uranyl: from disproportionation intermediates to stable clusters, *Chem. – Eur. J.*, 2010, **16**, 14365–14377.

19 M. J. Sarsfield and M. Helliwell, Extending the chemistry of the uranyl ion: Lewis acid coordination to a UO oxygen, *J. Am. Chem. Soc.*, 2004, **126**, 1036–1037.

20 (*a*) D. D. Schnaars, G. Wu and T. W. Hayton, Reduction of pentavalent uranyl to U (IV) facilitated by oxo functionalization, *J. Am. Chem. Soc.*, 2009, **131**, 17532–17533; (*b*) T. W. Hayton and G. Wu, Exploring the Effects of Reduction or Lewis Acid Coordination on the U=O Bond of the Uranyl Moiety, *Inorg. Chem.*, 2009, **48**, 3065–3072.

21 R. R. Golwankar, M. Z. Makoś, N. Cajiao, M. L. Neidig, A. G. Oliver, C. S. Day, V. W. Day, V.-A. Glezakou and J. D. Blakemore, Activation and Functionalization of the Uranyl Ion by Electrochemical Reduction, *Inorg. Chem.*, 2024, **63**, 24542–24553.

22 E. R. Mikeska, M. Z. Makoś, G. A. Arehart, V.-A. Glezakou and J. D. Blakemore, Distinguishing Desirable and Undesirable Reactions in Multicomponent Systems for Redox Activation of the Uranyl Ion, *Inorg. Chem.*, 2025, **64**, 5827–5845.

23 C. J. Pedersen, Cyclic polyethers and their complexes with metal salts, *J. Am. Chem. Soc.*, 1967, **89**, 7017–7036.

24 A. H. Reath, J. W. Ziller, C. Tsay, A. J. Ryan and J. Y. Yang, Redox Potential and Electronic Structure Effects of Proximal Nonredox Active Cations in Cobalt Schiff Base Complexes, *Inorg. Chem.*, 2017, **56**, 3713–3718.

25 (*a*) J. R. Robinson, P. J. Carroll, P. J. Walsh and E. J. Schelter, The impact of ligand reorganization on cerium(III) oxidation chemistry, *Angew. Chem., Int. Ed.*, 2012, **40**, 10159–10163; (*b*) J. R. Robinson, Z. Gordon, C. H. Booth, P. J. Carroll, P. J. Walsh and E. J. Schelter, Tuning reactivity and electronic properties through ligand reorganization within a cerium heterobimetallic framework, *J. Am. Chem. Soc.*, 2013, **135**, 19016–19024; (*c*) N. T. Rice, J. Su, T. P. Gompa, D. R. Russo, J. Telser, L. Palatinus, J. Bacsa, P. Yang, E. R. Batista and H. S. La Pierre, Homoleptic imidophosphorane stabilization of tetravalent cerium, *Inorg. Chem.*, 2019, **58**, 5289–5304.

26 (*a*) G. Milburn, M. R. Truter and B. Vickery, The crystal structure of a sodium complex, sodium perchlorate–bis-[NN′-ethylenebis (salicylideneiminato) copper(II)], *Chem. Commun.*, 1968, 1188–1188; (*b*) M. R. Truter, in *Alkali Metal Complexes with Organic Ligands*, Springer, 2005, pp. 71–111; (*c*) C. Floriani, F. Calderazzo and L. Randaccio, Crystal and molecular structure of a cationic sodium complex: the sodium tetraphenylborate adduct of NN′-ethylenebis (salicylideneiminato) cobalt(II). Cobalt(II), nickel(II), and copper(II) complexes of quadridentate Schiff bases as complexing agents for lithium, sodium, and ammonium cations, *J. Chem. Soc., Chem. Commun.*, 1973, 384–385.

27 (*a*) B. Guillaume, G. Begun and R. Hahn, Raman spectrometric studies of" cation-cation" complexes of pentavalent actinides in aqueous perchlorate solutions, *Inorg. Chem.*, 1982, **21**, 1159–1166; (*b*) G. Lu, T. Z. Forbes and A. J. Haes, Evaluating best practices in Raman spectral analysis for uranium speciation and relative abundance in aqueous solutions, *Anal. Chem.*, 2016, **88**, 773–780; (*c*) M. Autillo, R. E. Wilson, M. Vasiliu, G. F. de Melo and D. A. Dixon, Periodic Trends within Actinyl (VI) Nitrates and Their Structures, Vibrational Spectra, and Electronic Properties, *Inorg. Chem.*, 2022, **61**, 15607–15618; (*d*) J. Bullock, Raman and infrared spectroscopic studies of the uranyl ion: the symmetric stretching frequency, force constants, and bond lengths, *J. Chem. Soc. A*, 1969, 781–784.

28 (*a*) L. H. Jones and R. A. Penneman, Infrared Spectra and Structure of Uranyl and Transuranium(V) and (VI) Ions in Aqueous Perchloric Acid Solution, *J. Chem. Phys.*, 1953, **21**, 542–544; (*b*) L. H. Jones, Systematics in the vibrational spectra of uranyl complexes, *Spectrochim. Acta*, 1958, **10**, 395–403; (*c*) L. H. Jones, Determination of U-O bond distance in uranyl complexes from their infrared spectra, *Spectrochim. Acta*, 1959, **15**, 409–411.

29 (*a*) D. D. Schnaars and R. E. Wilson, Structural and Vibrational Properties of $U(VI)O_2Cl_4^{2-}$ and $Pu(VI)O_2Cl_4^{2-}$ Complexes, *Inorg. Chem.*, 2013, **52**, 14138–14147; (*b*) D. D. Schnaars and R. E. Wilson, Lattice Solvent and Crystal Phase Effects on the Vibrational Spectra of $UO_2Cl_4^{2-}$, *Inorg. Chem.*, 2014, **53**, 11036–11045; (*c*) D. D. Schnaars and R. E. Wilson, Synthesis, Structure, and Vibrational Properties of $[Ph_4P]_2NpO_2Cl_4$ and $[Ph_4P]_2PuO_2Cl_4$ Complexes, *Inorg. Chem.*, 2018, **57**, 3008–3016; (*d*) M. Autillo, R. E. Wilson, M. Vasiliu, G. F. de Melo and D. A. Dixon, Periodic Trends within Actinyl(VI) Nitrates and Their Structures, Vibrational Spectra, and Electronic Properties, *Inorg. Chem.*, 2022, **61**, 15607–15618.

30 (*a*) R. G. Surbella III, L. C. Ducati, K. L. Pellegrini, B. K. McNamara, J. Autschbach, J. M. Schwantes and C. L. Cahill, Transuranic Hybrid Materials: Crystallographic and Computational Metrics of Supramolecular Assembly, *J. Am. Chem. Soc.*, 2017, **139**, 10843–10855; (*b*) K. P. Carter, M. Kalaj, R. G. Surbella III, L. C. Ducati, J. Autschbach and C. L. Cahill, Engaging the Terminal: Promoting Halogen Bonding Interactions with Uranyl Oxo Atoms, *Chem. – Eur. J.*, 2017, **23**, 15355–15369; (*c*) K. P. Carter, M. Kalaj, A. Kerridge and C. L. Cahill, Probing hydrogen and halogen-oxo interactions in uranyl coordination polymers: a combined crystallographic and computational study, *CrystEngComm*, 2018, **20**, 4916–4925.

31 (*a*) M. Basile, E. Cole and T. Z. Forbes, Impacts of Oxo Interactions on Np(V) Crown Ether Complexes, *Inorg. Chem.*, 2018, **57**, 6016–6028; (*b*) J. L. Bjorklund, M. M. Pyrch, M. C. Basile, S. E. Mason and T. Z. Forbes, Actinyl-cation interactions: experimental and theoretical assessment of $[Np(VI)O_2Cl_4]^{2-}$ and $[U(VI)O_2Cl_4]^{2-}$ systems, *Dalton Trans.*, 2019, **48**, 8861–8871.

32 (*a*) C. J. Van Staveren, D. E. Fenton, D. N. Reinhoudt, J. Van Eerden and S. Harkema, Co-complexation of urea and $UO_2^{2+}$ in a Schiff base macrocycle: a mimic of an enzyme binding site, *J. Am. Chem. Soc.*, 1987, **109**, 3456–3458; (*b*) C. J. Van Staveren, J. Van Eerden, F. C. Van Veggel, S. Harkema and D. N. Reinhoudt, Cocomplexation of

 This journal is © The Royal Society of Chemistry 2025

Open Access Article. Published on 12 March 2025. Downloaded on 6/5/2026 2:38:04 PM. This article is licensed under a Creative Commons Attribution-NonCommercial 3.0 Unported Licence.

neutral guests and electrophilic metal cations in synthetic macrocyclic hosts, *J. Am. Chem. Soc.*, 1988, **110**, 4994–5008.

33 (*a*) P. Zanello, A. Cinquantini, P. Guerriero, S. Tamburini and P. Vigato, Electrochemical behaviour of acyclic and macrocyclic complexes of nickel(II), copper(II) and uranyl (VI), *Inorg. Chim. Acta*, 1986, **117**, 91–96; (*b*) U. Casellato, S. Tamburini, P. Tomasin, P. A. Vigato, S. Aime and M. Botta, Synthesis, X-ray structure, and solution NMR studies of Ln(III) complexes with a macrocyclic asymmetric compartmental Schiff base. Preference of the Ln(III) ions for a crown-like coordination site, *Inorg. Chem.*, 1999, **38**, 2906–2916; (*c*) N. Brianese, U. Casellato, S. Tamburini, P. Tomasin and P. Vigato, Asymmetric compartmental macrocyclic ligands and related mononuclear and heterodinuclear complexes with d-and/or f-metal ions, *Inorg. Chim. Acta*, 1999, **293**, 178–194; (*d*) U. Casellato, S. Tamburini, P. Tomasin and P. Vigato, Uranyl (VI) complexes with [1 + 1] asymmetric compartmental ligands containing a Schiff base and a crown ether-like chamber, *Inorg. Chim. Acta*, 2002, **341**, 118–126.

34 (*a*) R. D. Shannon and C. Prewitt, Revised values of effective ionic radii, *Acta Crystallogr., Sect. B*, 1970, **26**, 1046–1048; (*b*) R. D. Shannon, Revised effective ionic radii and systematic studies of interatomic distances in halides and chalcogenides, *Acta Crystallogr., Sect. A*, 1976, **32**, 751–767.

35 T. Makela, M.-E. Minkkinen and K. Rissanen, Ion pair binding in the solid-state with ditopic crown ether uranyl salophen receptors, *Inorg. Chem.*, 2016, **55**, 1339–1346.

36 A. Kumar, D. Lionetti, V. W. Day and J. D. Blakemore, *CCDC 1960629: Experimental Crystal Structure Determination*, 2020, DOI: **10.5517/ccdc.csd.cc23t638**.

37 A. Kumar, D. Lionetti, V. W. Day and J. D. Blakemore, *CCDC 1960628: Experimental Crystal Structure Determination*, 2020, DOI: **10.5517/ccdc.csd.cc23t627**.

38 J.-M. Savéant, *Elements of Molecular and Biomolecular Electrochemistry*, Wiley-VCH, New Jersey, 2006.

39 A. Kumar and J. D. Blakemore, On the Use of Aqueous Metal-Aqua p$K_a$ Values as a Descriptor of Lewis Acidity, *Inorg. Chem.*, 2021, **60**, 1107–1115.

40 D. D. Perrin, *Ionisation Constants of Inorganic Acids and Bases in Aqueous Solution*, Elsevier, 2016.

41 R. S. Nicholson, Theory and application of cyclic voltammetry for measurement of electrode reaction kinetics, *Anal. Chem.*, 1965, **37**, 1351–1355.

42 A. J. Bard and L. R. Faulkner, *Electrochemistry: Fundamentals and Applications*, John Wiley and Sons Inc., Hoboken, 2nd edn, 2001.

43 P. Thordarson, Determining association constants from titration experiments in supramolecular chemistry, *Chem. Soc. Rev.*, 2011, **40**, 1305–1323.

44 G. Salinas, A. Villarroel Marquez, M. Idir, S. Shinde, B. A. Frontana-Uribe, M. Raoux, J. Lang, E. Cloutet and A. Kuhn, Sodium-Ion Selectivity Study of a Crown-Ether-Functionalized PEDOT Analog, *ChemElectroChem*, 2020, **7**, 2826–2830.

45 J. D. Blakemore, R. Chitta and F. D'Souza, Synthesis and study of crown ether-appended boron dipyrrin chemosensors for cation detection, *Tetrahedron Lett.*, 2007, **48**, 1977–1982.

46 G. Wulfsberg, *Principles of Descriptive Inorganic Chemistry*, University Science Books, Mill Valley, Calif., 1991.

47 J. E. Newbery, Vibrational spectra of the $[UO_2Cl_4]^{2-}$ and the $[UO_2Br_4]^{2-}$ ions, *Spectrochim. Acta, Part A*, 1969, **25**, 1699–1702.